Complexities of the San Andreas fault near San Gorgonio Pass: Implications for large earthquakes

Doug Yule[1] and Kerry Sieh

Seismological Laboratory, California Institute of Technology, Pasadena, California, USA

Received 13 February 2001; revised 30 December 2002; accepted 27 February 2003; published 29 November 2003.

[1] Geologic relationships and patterns of crustal seismicity constrain the three-dimensional geometry of the active portions of San Andreas fault zone near San Gorgonio Pass, southern California. Within a 20-km-wide contractional stepover between two segments of the fault zone, the San Bernardino and Coachella Valley segments, folds, and dextral-reverse and dextral-normal faults form an east-west belt of active structures. The dominant active structure within the stepover is the San Gorgonio Pass-Garnet Hill faults, a dextral-reverse fault system that dips moderately northward. Within the hanging wall block of the San Gorgonio Pass-Garnet Hill fault system are subsidiary active dextral and dextral-normal faults. These faults relate in complex but understandable ways to the strike-slip faults that bound the stepover. The pattern of crustal seismicity beneath these structures includes a 5–8 km high east-west striking step in the base of crustal seismicity, which corresponds to the downdip limit of rupture of the 1986 North Palm Springs earthquake. We infer that this step has been produced by slip on the linked San Gorgonio Pass-Garnet Hill-Coachella Valley Banning (SGP-GH-CVB) fault. This association enables us to construct a structure contour map of the fault plane. The large step in the base of seismicity downdip from the SGP-GH-CVB fault system probably reflects a several kilometers offset of the midcrustal brittle-plastic transition. (U/Th)/He thermochronometry supports our interpretation that this south-under-north thickening of the crust has created the region's 3 km of topographic relief. We conclude that future large earthquakes generated along the San Andreas fault in this region will have a multiplicity of mostly specifiable sources having dimensions of 1–20 km. Two tasks in seismic hazard evaluation may now be attempted with greater confidence: first, the construction of synthetic seismograms that make useful predictions of ground shaking, and second, theoretical investigations of the role of this complexity in retarding the propagation of future seismic ruptures. *INDEX TERMS:* 8102 Tectonophysics: Continental contractional orogenic belts; 8105 Tectonophysics: Continental margins and sedimentary basins (1212); 8107 Tectonophysics: Continental neotectonics; 8110 Tectonophysics: Continental tectonics—general (0905); 8115 Tectonophysics: Core processes (1507); 8124 Tectonophysics: Earth's interior—composition and state (1212); *KEYWORDS:* San Andreas fault zone, San Gorgonio Pass, neotectonics, three-dimensional fault geometry, transpression, fault interaction

Citation: Yule, D., and K. Sieh, Complexities of the San Andreas fault near San Gorgonio Pass: Implications for large earthquakes, *J. Geophys. Res.*, *108*(B11), 2548, doi:10.1029/2001JB000451, 2003.

1. Introduction

[2] Discontinuities of crustal dimension are rare along the 1100-km length of the San Andreas fault (Figure 1, inset). This scarcity of large structural irregularities may, in fact, encourage lengthy seismic ruptures like the 360- and 420-km-long events of 1857 and 1906 [*Sieh*, 1978], since geometrical complexities appear to play a critical role in impeding rupture propagation [for example, *Barka and Kadinsky-Cade*, 1988; *Harris and Day*, 1993; *Wesnousky and Jones*, 1994; *Rice and Ben-Zion*, 1996; *Sieh and Natawidjaja*, 2000]. The largest irregularity in the San Andreas fault occurs in southern California, in the vicinity of San Gorgonio Pass (Figure 1). Here at a contractional left step [*Matti et al.*, 1985, 1992a; *Matti and Morton*, 1993], the surface trace of the San Andreas fault disaggregates into a family of irregular and discontinuous faults [*Allen*, 1957; *Dibblee*, 1968, 1982; *Hill*, 1982; *Matti et al.*, 1985, 1992a; *Matti and Morton*, 1993].

[3] The exceptional complexity of the San Andreas fault zone in the region of San Gorgonio Pass, southern California, presents a formidable challenge to forecasting the source characteristics of future earthquakes there. Recent earthquakes in structurally complex regions provide two general insights, however. First, the nearly synchronous failure of several faults can lead to unusually complex earthquakes. The complex Spitak, Armenia, earthquake of

[1]Now at Department of Geological Sciences, California State University, Northridge, California, USA.

0148-0227/03/2001JB000451$09.00

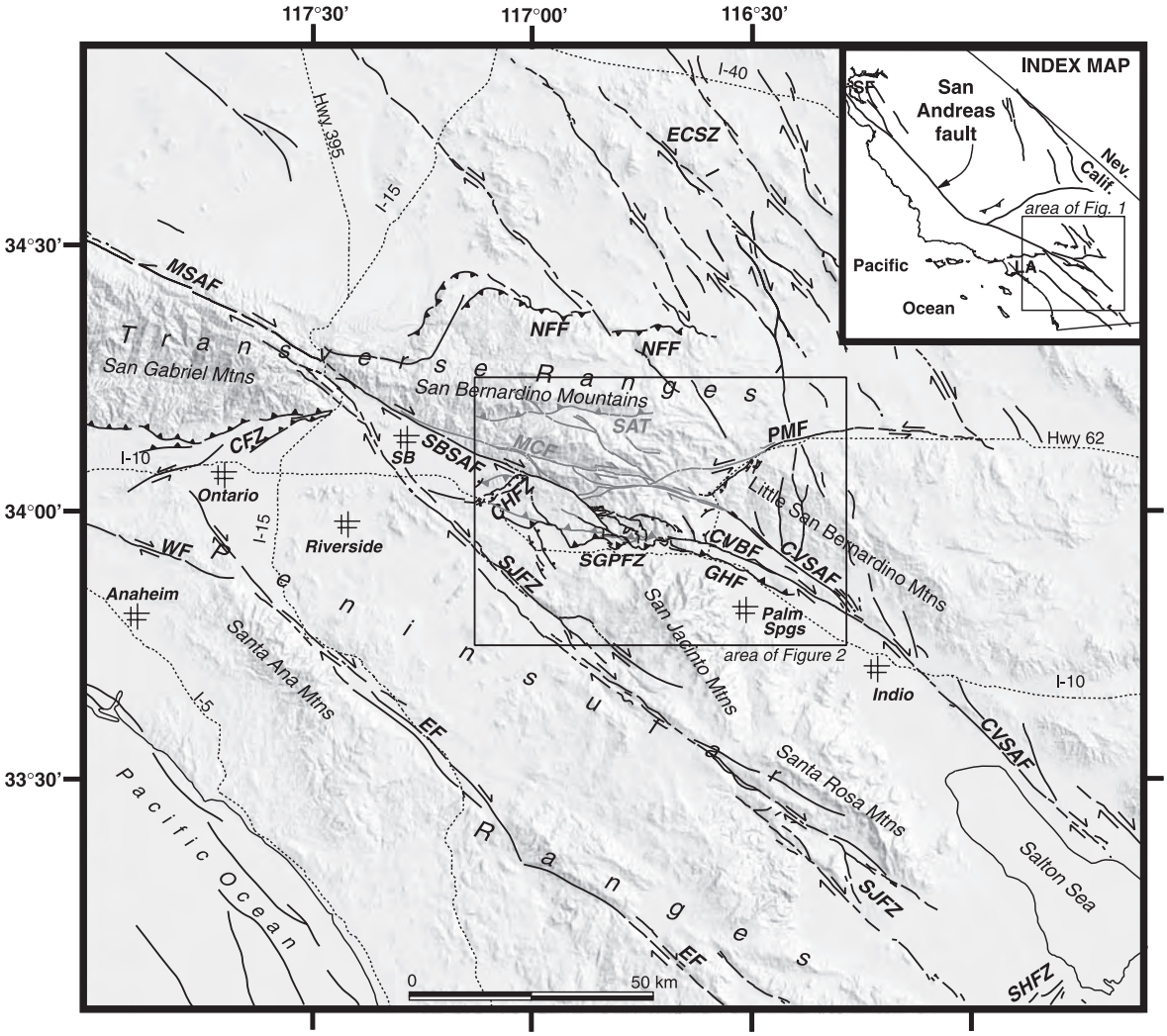

Figure 1. Shaded topographic relief map of the eastern Transverse Ranges and northern Peninsular Ranges, southern California, showing Holocene faults in black. Late Pleistocene faults in the vicinity of San Gorgonio Pass, considered inactive, in gray. Abbreviations: CFZ, Cucamonga fault zone; CHFZ, Crafton Hills fault zone; CVBF, Coachella Valley segment Banning fault; CVSAF, Coachella Valley segment, San Andreas fault; EF, Elsinore fault; ECSZ, eastern California shear zone; GHF, Garnet Hill fault; MCF, Mill Creek fault; MSAF, Mojave segment, San Andreas fault; NFF, north frontal fault; PMF, Pinto Mountain fault; SAT, Santa Ana thrust; SBSAF, San Bernardino strand, San Andreas fault; SGPFZ, San Gorgonio Pass fault zone; SHFZ, Superstition Hills fault zone; SJFZ, San Jacinto fault zone; and WF, Whittier fault; SB, San Bernardino; LA, Los Angeles; SF, San Francisco.

1988, for example, was caused by sequential rupture of adjacent strike-slip, thrust, and blind thrust faults [*Cisternas et al.*, 1989]. The complicated Landers, California, earthquake of 1992 was also produced by sequential rupture of several strike-slip faults [*Sieh et al.*, 1993; *Wald and Heaton*, 1994]. Second, relatively simple faults within structurally complex regions may be unrecognized prior to failure in destructive earthquakes. The source of the 1989 *M*7.1 Loma Prieta earthquake, for example, was a simple but hidden, moderately dipping, dextral-reverse fault beneath a large contractional jog in the San Andreas fault in the southern San Francisco Bay region [*Lisowski et al.*, 1990; *Marshall et al.*, 1991; *Anderson*, 1994]. Likewise, the dip and dextral-reverse sense of slip on a portion of the San Andreas fault zone north of Palm Springs was underappreciated until the occurrence of a moderate earthquake in 1986 [*Hartzell*, 1989; *Jones et al.*, 1986].

[4] Some basis exists therefore for speculation that past and future ruptures of the San Andreas fault through the San Gorgonio Pass region have been and will be complex and surprising. In addition, some have speculated that the structural complexity will impede or terminate rupture [for example, *Sykes and Seeber*, 1985].

[5] But beyond these broad, general expectations, what can we say about the past and future behavior of the fault zone? In this paper, we attempt to gain a more specific understanding of the San Andreas fault's seismic potential through new geologic mapping and a kinematic analysis of the active

structures. We integrate these data with upper crustal seismicity [*Jones et al.*, 1986; *Seeber and Armbruster*, 1995; *Magistrale and Sanders*, 1996] and present a plausible three-dimensional configuration of the brittle crust through the San Gorgonio Pass stepover. Our model, modified from that of *Matti et al.* [1985, 1992a] and *Matti and Morton* [1993], depicts the San Gorgonio Pass region as a south-under-north restraining ''bend'' in the San Andreas fault zone, with dextral-oblique strain broadly distributed on a family of faults and folds. This integrated view of the available geologic and geophysical data provides a basis for our construction of realistic seismic source models.

2. Overview of Active Structures

[6] *Vaughan* [1922] first showed the general distribution of rock units in the area, but did not recognize that many of the contacts are faults. *Noble* [1926, 1932] observed that the San Andreas splays into several branches in this region. *Allen* [1957] mapped most of the important faults and added critical details about sedimentary history. Particularly important were his recognition of the Banning fault and demonstration of its dextral-reverse character. *Matti et al.* [1985, 1992a] and *Matti and Morton* [1993] produced synoptic maps of active structures within the region and emphasized the significance of the contractional left stepover in the San Andreas fault and the major role currently being played by the active dextral-reverse San Gorgonio Pass fault (SGPF) system.

[7] We have modified the earlier mapping of the stepover region, paying particular attention to determination of which structures are active and which are not. Active structures possess one or more of the following characteristics: fault scarps in Holocene alluvium or steep scarps in older units, deflected drainages, offset ridgelines, and deformed late Quaternary surfaces. Inactive structures do not meet any or most of these criteria. By these criteria, we find that some faults have both active and inactive segments. Except where noted, we adopt the nomenclature of *Matti et al.* [1985, 1992a] and *Matti and Morton* [1993] for the primary faults and of *Allen* [1957] for the secondary structures.

[8] Figure 2 provides a synoptic view of the active structures that comprise the San Gorgonio Pass stepover region, superimposed on topography. We define the San Gorgonio Pass stepover as a 20-km-wide left stepover between the right-lateral strike-slip San Bernardino and Coachella Valley strands of the San Andreas fault (Figure 2). Other faults in the region act to transfer slip across the stepover. The right-oblique, San Gorgonio Pass thrust and Garnet Hill reverse faults bound the stepover on the south; the SGPF system extends westward beyond the stepover (Figure 2a). A system of right-oblique normal faults dominates the active structures within the hanging wall block of the stepover. Active local and regional scale folds are also important within the region (Figure 2b). Slip transfer in the stepover region is addressed in later sections. Below, we describe in general each of these active folds and fault zones by class, and then focus in detail on two small areas to illustrate the nature of the structures more fully.

2.1. Bounding Right-Lateral Strike-Slip Faults

[9] The ''San Bernardino strand, San Andreas fault'' bounds the San Gorgonio stepover on the west. Northwest of the stepover region, near Yucaipa (Figure 2a), it displays clear geomorphic and stratigraphic evidence of recent strike-slip movement [for example, see *Harden and Matti*, 1989]. Here (U-Th)/He thermochronometry appears to show that the fault's steep SSW-facing escarpment (Figure 2a) formed about 1.5 Ma ago [*Spotila et al.*, 1998]. Both large and small landforms diminish in their geomorphic expression southeastward from Yucaipa, along the western flank of the stepover. At San Gorgonio Canyon the fault experiences a pronounced southward bend, breaks into discontinuous right-stepping segments, and may die out southeast of Burro Flats [*Matti et al.*, 1985, 1992a; *Matti and Morton*, 1993] where its geomorphic expression is obscure (Figures 2a and 3a). However, subtle pressure ridges and hanging valleys along the southwest edge of Potrero Canyon suggest that the fault continues and merges with the Gandy Ranch fault (Figures 2a and 3a). The broadly linear trace of the fault between San Gorgonio and Potrero Canyons suggests that its dip is steep, but surface exposures are poor, so this has not been verified by direct measurement. A recent excavation at Burro Flats does, however, show the fault dipping 75° southwest [*Yule et al.*, 2001].

[10] The ''Coachella Valley segments of the Banning (CVB) and San Andreas (CVSA) faults'' diverge from one another and bend toward the west as they approach the San Gorgonio Pass stepover from the southeast. The active trace of the CVB fault merges with the SGPF at Cottonwood Canyon, and the active trace of the CVSA fault appears to end at Hwy 62 [*Matti et al.*, 1985, 1992a, Figure 2a]. The CVSA fault bifurcates into the Mill Creek and Mission Creek faults northwest of Hwy 62, but evidence for Holocene offset on these structures is equivocal. Farther to the southeast the CVSA faults exhibit clear Holocene scarps, laterally offset landforms, deformed adjacent young alluvial surfaces, and vegetation alignments [*Allen*, 1957; *Keller et al.*, 1982; *Clark*, 1984], and the CVB displays these features all the way into San Gorgonio Pass.

2.2. Right-Oblique Contractional Structures

[11] Right-oblique contractional structures skirt the southern boundary of the San Gorgonio Pass stepover. These constitute the San Gorgonio Pass and Garnet Hill faults (Figures 2a and 3).

[12] The ''San Gorgonio Pass fault'' exhibits an irregular sawtooth shape. Generally, east to northeast-trending thrust faults alternate with northwest-trending tears [*Matti et al.*, 1985, 1992a; *Matti and Morton*, 1993] (Figures 2a and 3a). West of Deep Canyon (Figure 3a), the fault trace is well defined by small scarps in late Holocene alluvium. Three lobes of deformed Pleistocene alluvium east of Deep Canyon indicate that the underlying fault has a scalloped geometry (Figure 3a). But the amplitude of the scalloping is uncertain, due to erosion or burial of the fault trace in the two large intervening canyons. Scarps in late Holocene alluvium occur only very locally, principally in locations that are sheltered from the rapid deposition and erosion that occurs at the mouths of major canyons.

[13] Traces of the ''Banning fault'' appear to be inactive along most of the fault's length, with the exception of one segment at Millard Canyon (Figure 3). A scarp in late Holocene alluvium across the valley floor and offset of late Quaternary fluvial gravels demonstrate its activity there. But

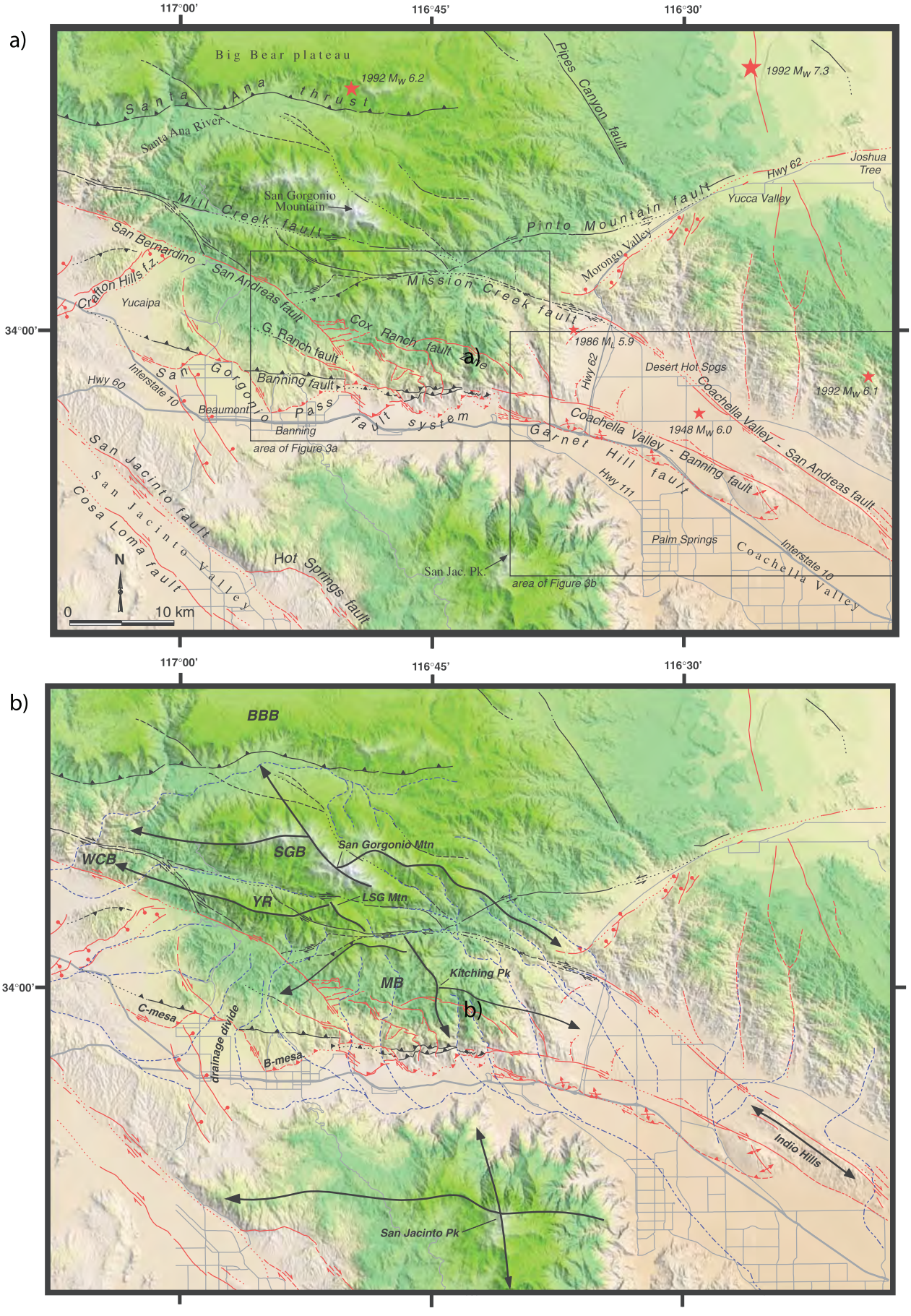
a)
117°00'
116°45'
116°30'
34°00'
Big Bear plateau
Santa Ana thrust
1992 Mw 6.2
1992 Mw 7.3
Santa Ana River
Pipes Canyon fault
Joshua Tree
Hwy 62
Yucca Valley
San Gorgonio Mountain
Mill Creek fault
Pinto Mountain fault
Morongo Valley
San Bernardino - San Andreas fault
Crafton Hills f.z.
Yucaipa
Mission Creek fault
Cox Ranch fault
G. Ranch fault
1986 ML 5.9
Desert Hot Spgs
Hwy 60
Interstate 10
San Gorgonio Pass fault system
Banning fault
Beaumont
Banning
area of Figure 3a
1948 Mw 6.0
1992 Mw 6.1
Coachella Valley - San Andreas fault
Garnet Hill fault
Coachella Valley - Banning fault
Hwy 111
San Jacinto fault
San Jacinto Valley
Cosa Loma fault
Hot Springs fault
San Jac. Pk.
area of Figure 3b
Palm Springs
Interstate 10
Coachella Valley
N
0
10 km
b)
BBB
SGB
WCB
YR
San Gorgonio Mtn
LSG Mtn
MB
Kitching Pk
C-mesa
drainage divide
B-mesa
Indio Hills
San Jacinto Pk

the absence of geomorphic or stratigraphic evidence of young offsets in the next canyon to the east (Deep Canyon) suggests that slip transfers to another structure between Millard and Deep Canyons.

[14] The active portion of the "Gandy Ranch fault" is marked by up-on-the-north, west-northwest trending scarps in young alluvium at the mouth of Potrero Canyon (Figure 3). The fault also places crystalline rocks over late Quaternary gravels between Potrero and Millard Canyons. The Gandy Ranch fault appears to merge with the active segment of the Banning fault.

[15] The "Garnet Hill fault" consists of a series of left-stepping, northwest-trending right-lateral faults with active folds at each stepover. Amplitudes and axial trends define two types of folds. Those at the eastern and western ends of the fault, marked by Edom Hill and West Whitewater Hill, show about 400 m of relief and north- to northwest-trending axes (Figure 3b). These larger folds at the end of the fault are manifestations of the transfer of slip from the Coachella Valley strand of the Banning fault onto the Garnet Hill fault. Folds at stepovers along the fault, marked by Garnet Hill, "Hugo" Hill, and East Whitewater Hill are much smaller. They show only 30–200 m of relief and east-trending axes. These smaller folds result from contractional, en echelon stepovers in the fault trace. The discontinuous geometry of the Garnet Hill fault and the small size of these folds suggest that cumulative slip is too low to have led yet to integration of the fault into a single strand.

2.3. Right-Oblique Normal Faults

[16] *Allen* [1957] applied the name "Cox Ranch fault" to a 10-km fault segment cutting crystalline basement rocks to the north of the SGPF (Figures 2a and 3a). We group this fault with a series of similar, unnamed faults mapped by *Allen* [1957] and by ourselves, and refer to them as the "Cox Ranch fault zone." These arcuate structures strike predominantly west-northwest to east-west with the exception of a few short north-south striking faults. They offset ridgelines and show faceted surfaces and slickensides, but do not show obvious scarps where they cross Holocene alluvium. This is an indication that rates of slip on these structures are small, relative to the other structures in the region.

[17] These structures show variable orientations and offsets. For example, the Cox Ranch fault and a subparallel set of discontinuous faults to the south and southwest show dextral-normal ridgeline offsets (Figures 3a and 4). In contrast, faults in and near Burro Flats comprise an asymmetric, intramontane graben with both down-to-the-north and down-to-the-south, primarily dip-slip displacements (Figures 3a and 5). North-trending faults about a kilometer east of Millard Canyon define another intramontane graben (Figure 3a). Estimates of displacement across individual faults, based on offset ridges, range from tens of meters to 250 m of dextral offset and tens of meters to 100 meters of vertical offset. Cumulative offset across the Cox Ranch fault system, since inception of the current topography, equals 250–500 m of dextral offset and 150–250 m of normal (down-to-the-south) offset.

2.4. Normal Faults

[18] A series of discontinuous and overlapping, northeast-trending scarps with down-to-the-northwest displacement bound the southeastern margin of the Morongo Valley [*Matti et al.*, 1985, 1992a] (Figure 2a). Quaternary displacement on the "Morongo Valley fault" has therefore produced an intermontane valley that separates the San Bernardino and Little San Bernardino Mountains. In the northwestern Coachella Valley, similar northeast-trending late Quaternary scarps occur between the Coachella Valley segments of the San Andreas and Banning faults (Figure 3b). These scarps show northwest-down or northwest-up displacement, consistent with northwest-directed transtension in the greater Coachella Valley region [*Matti and Morton*, 1993].

3. Selected Details of Active Structures

[19] Having completed an overview of the active structures of the San Gorgonio Pass region, we will now focus on two localities where the geologic relationships are particularly illustrative of active neotectonic deformation. First, we consider young deformation near the mouth of Millard Canyon (Figure 3a). The relationship between thrust segments and lateral tears of the SGPF zone in this area is particularly important. Also, our mapping places important constraints on the relationship of the SGP fault zone to the dextral-slip faults that form the western edge of the San Gorgonio Pass stepover. Next, we examine young deformation near the mouths of Cottonwood and Whitewater Canyons (Figure 3a). Here also the relationship between strike-slip faults and thrust faults is particularly interesting and relevant.

3.1. Millard Canyon

[20] Figure 6 is a geologic map of the region around the mouth of Millard Canyon. Active faults (Holocene) appear in

Figure 2. (opposite) Synoptic view of the structures of the San Gorgonio Pass region (modified from *Matti et al.*, 1985, 1992a, 1992b and *Matti and Morton*, 1993), superimposed on topography. Both the Holocene (red) and late Pleistocene (black) structures between San Gorgonio and San Jacinto peaks show important relationships to the landforms of the San Bernardino Mountains. (a) Red stars indicate epicenters of significant earthquakes. Boxes show areas covered by Figures 3a and 3b. (b) Heavy dark lines with arrows marking large drainage divide approximate broad, regional flexures associated with crustal shortening at and near the stepover. Arrows point in direction of plunge. Dashed blue lines are streams and rivers that drain the south flank of the San Bernardino Mountains. Note that streams are deflected to the west and east of the central topographic highs, specifically San Gorgonio Mountain, Little San Gorgonio Mountain (LSG Mtn), and Kitching Peak. Streams draining the southwest flank of the Little San Bernardino Mountains are deflected to the northwest and southeast around the Indio Hills. Crustal blocks include: BBB, Big Bear block; SGB, San Gorgonio block; YR, Yucaipa Ridge; WCB, Wilson Creek block; and MB, Morongo block. Beaumont mesa (B-mesa) and Calimesa (C-mesa) are back-tilted late Pleistocene alluvial surfaces in the hanging wall of the SGPF system. Topographic base is shaded relief of a composite DEM image (10-m resolution) constructed from USGS 7.5′ quadrangle maps.

red and inactive faults (non-Holocene) appear in black. The principal "inactive" structures are strands of the east-west trending Banning fault. East of Millard Canyon, the northern strand places Cretaceous to pre-Cambrian crystalline rocks over Plio-Pleistocene sediments. The southern strands position Pliocene (Painted Hill and Hathaway Formations) sediments over late Pleistocene alluvial sands and gravels (Cabezon Formation). These traces merge into a solitary trace west of Millard Canyon. Although the black strands of the Banning fault were active after deposition of late Pleistocene

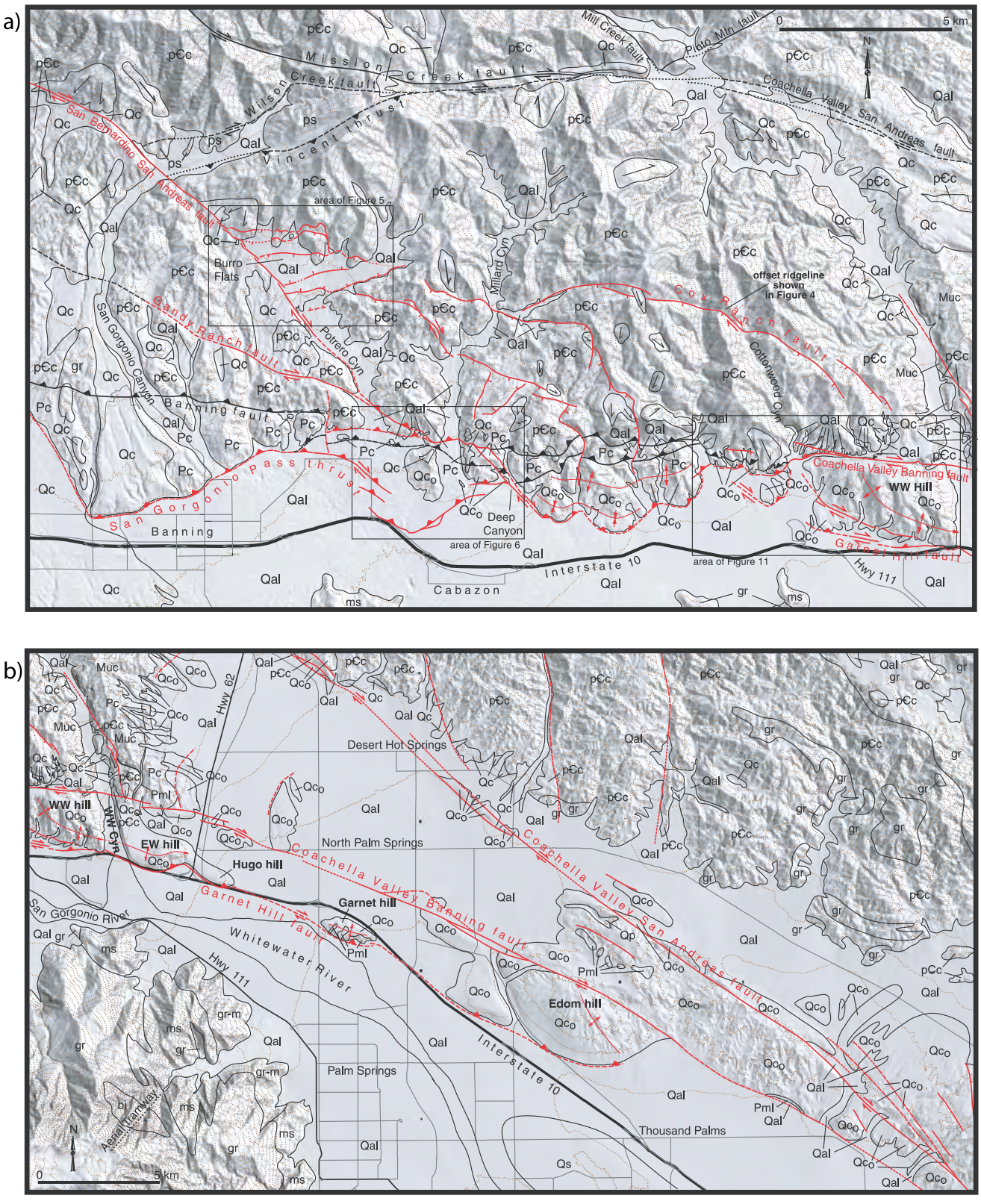

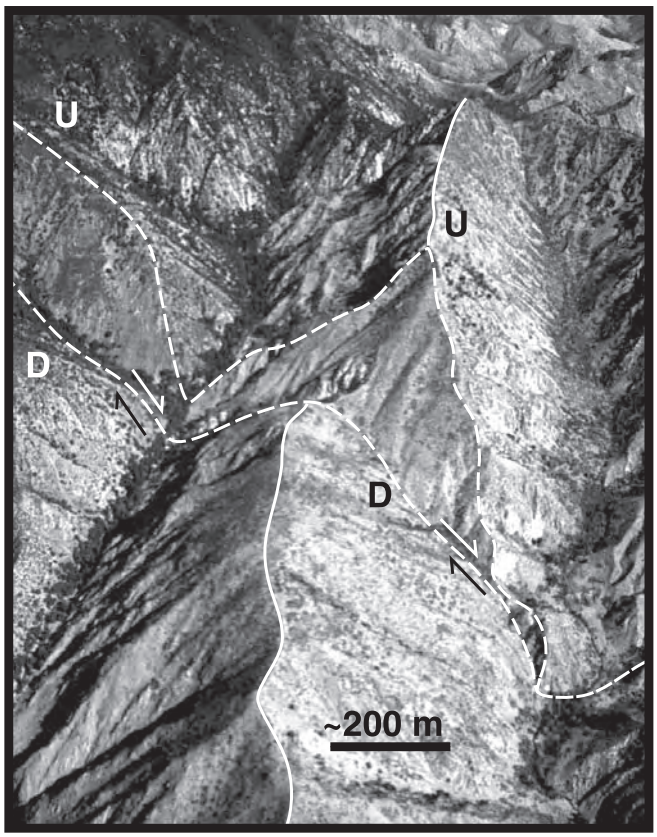

Figure 4. Oblique aerial view of scarp at an offset ridgeline along the Cox Ranch fault. Arrows indicate displacement. Up and downthrown sides are designated by U and D, respectively. View is northward from the ridgeline divide between Cottonwood and Stubbe Canyons. Trace of ridgeline shows ~200 m of dextral separation and ~100 m of vertical separation. See Figure 3a for location.

alluvial sands and gravels, an utter lack of geomorphic expression demonstrates that these strands are not currently active.

3.1.1. Banning Fault

[21] A 3-km-long segment of the northern strand of the Banning fault is, however, currently active at Millard Canyon (red portion in Figure 6). This section of the fault displays a 5-m-high scarp in Qf_3 (Qf, faulted alluvium; Qu, unfaulted alluvium), and a 2.5-m-high scarp in Qf_2 (Figure 7). Radiocarbon analysis of detrital charcoal within Qf_{1-2} indicates that it was deposited between about 2850 and 3600 radiocarbon years BP [J. C. Tinsley and J. C. Matti, in *Matti et al.*, 1992a, p. 26]. The base of the terrace riser that separates these two fluvial surfaces appears to be offset right-laterally about 4.5 m (Figure 8). Thus the dextral component of offset across the fault (1.3–1.6 mm/yr) appears to be about 80% greater than the vertical component (0.7–0.9 mm/yr).

[22] This active portion of the Banning fault also offsets the late Pleistocene heights fanglomerate several hundred meters. On the eastern wall of the canyon, the fault trace rises from the canyon floor at a dip of about 45° and juxtaposes crystalline rocks over the fanglomerate (Figures 6 and 9). Halfway up the canyon wall, the fault rolls over to a nearly horizontal dip and rides over the surface of the Heights fanglomerate.

[23] The age of this fluvial deposit (Qh) of Millard Canyon is poorly constrained. A deep reddish orange, clayey soil more than a meter thick atop the unit suggests that it is older than about 10^5 years, and the excellent preservation of remnants of its depositional surface suggests that it must be much less than 10^6 years old. Just east of the eastern wall of Millard Canyon, the Heights fanglomerate is plastered against an older eastern wall of the canyon, and this buttress unconformity is offset obliquely (Figure 6, inset). The base of the Heights buttress unconformity is exposed in six outcrops north of the fault and in two outcrops south of the fault. These allow us to constrain post-Heights offset of the Banning fault. Vertical offset is 140 ± 15 m, and dextral offset is 375 ± 75 m. The ratio of horizontal and vertical offset derived from these data is somewhat greater than that derived from the younger scarp on the valley floor. Nonetheless, both observations show that strike-slip offset exceeds dip-slip offset on this active section of the Banning fault. The post-Heights slip vector is about 480 m directed S59°E, nearly parallel to the strike of the San Bernardino strand of the San Andreas fault (Figure 2). Assuming an oldest plausible age of 100,000 years for the Heights surface, this strand of the fault zone accommodates a minimum of about 5 mm/yr of the

Figure 3. (opposite) Generalized geologic maps of (a) the central San Gorgonio Pass region and (b) the northern Coachella Valley superposed on topography. Late Pleistocene structural features, considered inactive, are black. Holocene structural features are red and include right-lateral, reverse, and normal-dextral faults (arrows, teeth, and ticks, respectively; teeth and ticks are in hanging wall of thrust and normal faults, respectively), and folds (hinge line, perpendicular arrows points in dip direction of limbs; parallel arrow points in plunge direction of fold). Rock units: Qal, Holocene alluvium; Qc, early Holocene and late Pleistocene alluvium, typically uplifted, back-tilted, and/or highly dissected; Qc_0, moderately deformed Late Pleistocene alluvium, including but not limited to the Cabezon Formation; Pc, strongly deformed Pliocene nonmarine deposits; Pml, lower Pliocene marine deposits of the Imperial Formation, exposed east of Whitewater Cyn; Muc, upper Miocene nonmarine deposits; gr, Mesozoic granitic rocks; bi, basic intrusive rock; ms, metasedimentary rocks; gr-m, granitic migmatite; pCc, undivided Cretaceous to pre-Cambrian igneous and metamorphic complex. Boxes show areas covered by Figures 5, 6, and 11. Contour interval = 100 m. Topographic base is shaded relief of a composite DEM (10-m resolution) constructed from USGS 7.5′ quadrangle maps [geology modified from *Allen*, 1957; *Dibblee*, 1964; 1970; *Matti et al.*, 1985, 1992a, 1992b; *Matti and Morton*, 1993, and J. C. Matti and D. M. Morton, 1991, unpublished mapping, Cabazon and Whitewater 7.5′ quadrangles].

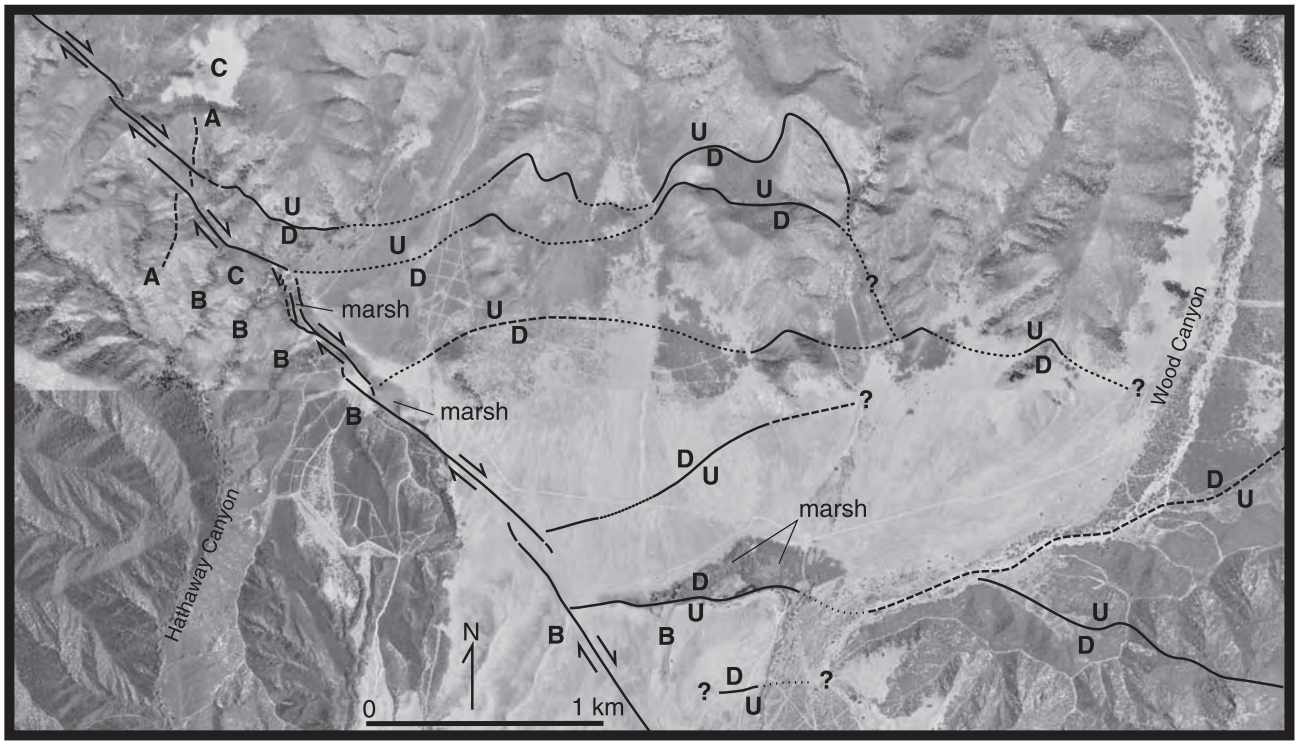

Figure 5. Orthophoto mosaic of the Burro Flats region showing the geomorphic expression of active structural features (see Figure 3a for location). The San Bernardino strand of the San Andreas fault crosses from upper left to middle bottom in a series of right-stepping segments. Marshes occur at some stepovers. Geomorphic features of the fault include A, a right-lateral offset ridgeline; B, beheaded stream channels; and C, uplifted and faulted alluvial surfaces (Qc of Figure 3a). The E-W striking fault segments are both down- and up-to-the-south strands of the western end of the Cox Ranch fault system and have produced the intermontane valley of Burro Flats. North- and south-facing scarps are locally preserved in Holocene alluvium. South-facing faceted slopes in crystalline bedrock characterize the northern strands. One of the southern strands acts as a barrier to groundwater forming the large marsh in the lower center of the photograph.

21–28 mm/yr [*Weldon and Sieh*, 1985] or of the 12–16 mm/yr [*Harden and Matti*, 1989] (0–90 ka best estimate) of dextral slip rate across the SAF zone near Cajon Pass and Yucaipa, 75 and 25 km to the northwest, respectively.

[24] Youthful offsets of the Heights fanglomerate are absent immediately east and west of this active segment of the Banning fault. To the east, slip may transfer off the Banning fault and onto faults at the mountain front via northwest-striking active faults. The total offset on these structures must, however, be no more than a few hundred meters, because separations of traces of the inactive Banning fault and on the axis of an anticline in the Pliocene Hathaway Fm are of this order (Figure 6). Northwest of Millard Canyon, slip appears to transfer off the Banning fault and onto the Gandy Ranch fault at a small right stepover where the two faults overlap between Millard and Potrero Canyons (Figures 3a and 6). Similarly, diminishing northwestward expression of the Gandy Ranch fault coupled with increasing northwestward expression of the San Bernardino strand of the San Andreas fault suggests that slip is transferred at a 2-km-wide right stepover between Potrero and San Gorgonio Canyons (Figure 3a). This right-stepping pattern can therefore explain how slip is transferred, via the Gandy Ranch and Banning faults, between the San Bernardino strand of the San Andreas fault and the SGPF zone (see below).

3.1.2. San Gorogonio Pass Fault Zone

[25] The SGPF zone forms a prominent northeast-trending scarp across the alluvial fan of Millard Canyon. Across Qf_1 the scarp is about 1.5-m high (Figure 10). In the western wall of the modern arroyo, the fault is well exposed in Qf_1 gravel and sand. Here it is a thrust fault zone that dips 24° northward in alluvial sand and gravel. The match of sand and gravel layers across the fault planes demonstrates that slip on the fault zone is nearly pure dip slip. Using the radiocarbon age of detrital charcoal contained within Qf_{1-2}, 2850–3600 radiocarbon years BP [J. C. Tinsley and J. C. Matti in *Matti et al.*, 1992a, p. 26], yields a minimum slip rate of 1.0–1.3 mm/yr and a horizontal contraction rate of about 0.9–1.2 mm/yr.

[26] The Qf_3 surface of Millard Canyon displays a scarp of about 3 m across the SGPF (Figure 10). Its age, however, is not well constrained. An older surface (Qf_4 on Figures 6 and 10) is offset about 12.5 m. This scarp must be a monoclinal flexure, rather than a fault scarp, because a small fluvial terrace riser traverses the scarp from the hanging wall block to the footwall block (hachured line in Qf_4 in Figure 6). The age

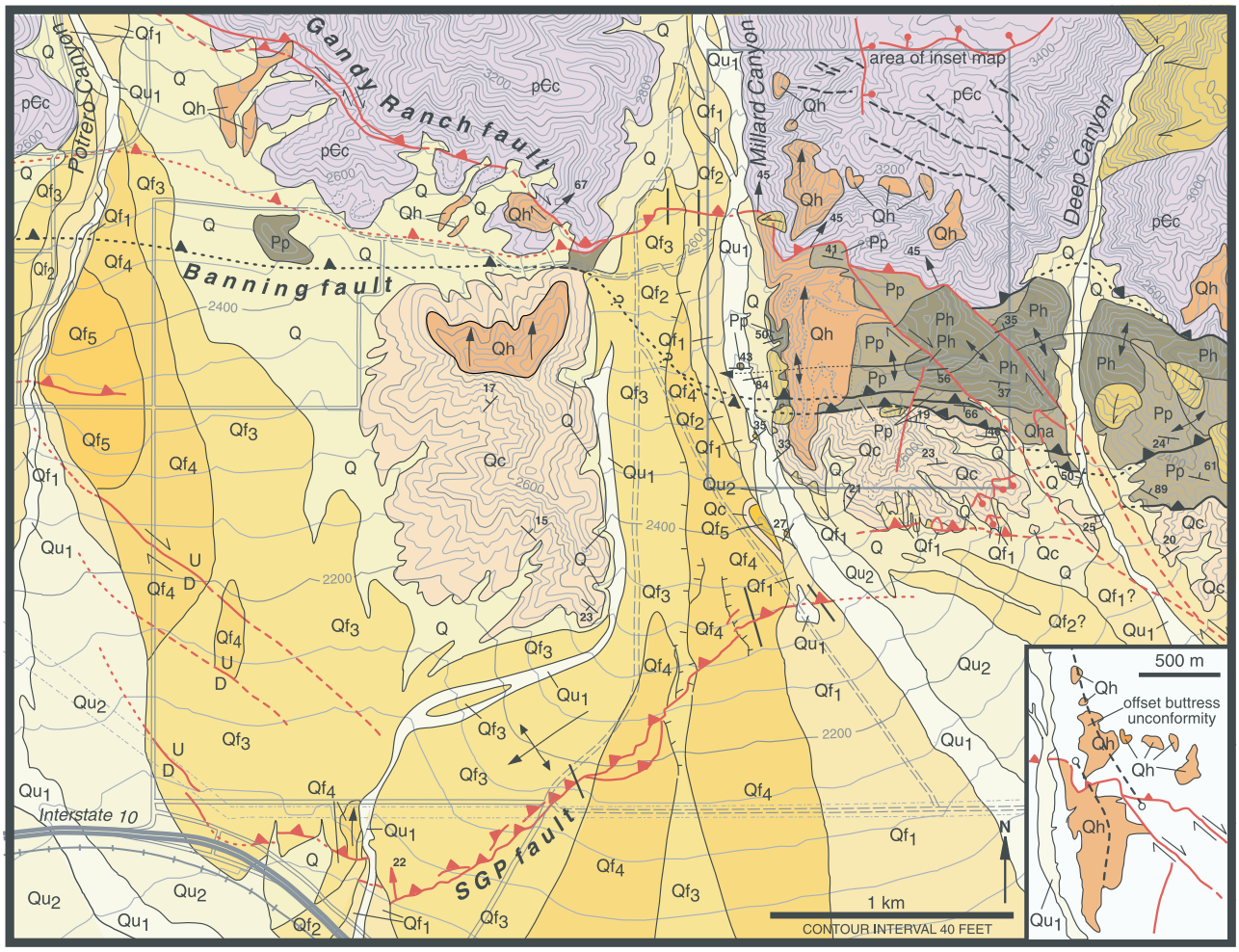

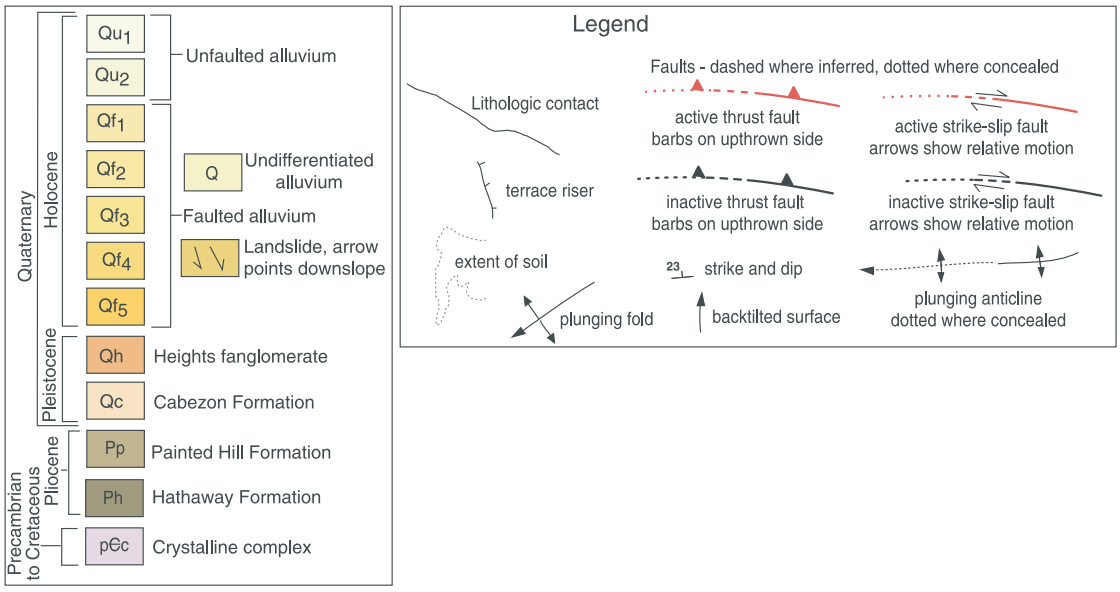

Figure 6. Geologic map of the Millard Canyon area (See Figure 3a for location). The San Gorgonio Pass and Banning fault zones consist of multiple, subparallel fault strands, some clearly active and others probably inactive. Scarps in Holocene alluvium are the clearest evidence for activity. Faults without preserved Holocene scarps or geomorphic evidence of recent slip are considered inactive. The San Bernardino strand, San Andreas fault merges with the SGPF zone just east of Millard Canyon. Black lines across the scarps in Millard Canyon represent surveyed profiles shown in Figures 7 and 10. The offset terrace riser, depicted on Figure 8, was surveyed between the two lines of profile shown across the northern scarp.

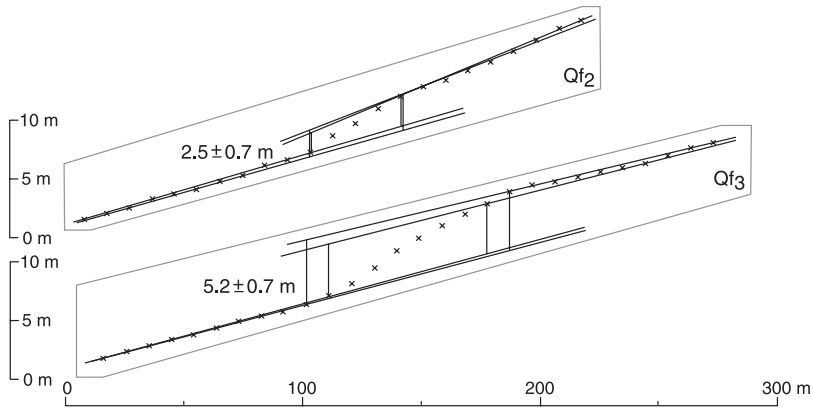

Figure 7. Cross-sectional view of surveyed profiles across the active segment of the Banning fault in Millard Canyon (see Figure 6 for locations of profiles). This scarp is 5.2 ± 0.7 m high in unit Qf_3 and 2.5 ± 0.7 m high in unit Qf_2. Vertical offsets were calculated taking the average of four measurements at the base and at the top of the scarp (see profiles). See text for discussion of slip-rate estimates based on these offsets.

of Qf_4 is also poorly known, but the poor degree of soil development suggests that it is no older than latest Pleistocene. We can estimate a shortening rate for the Qf_4 surface by assuming a latest Pleistocene age (<13,000 years) and a fault propagation fold geometry for the monocline, a reasonable assumption given that a 24° north-dipping thrust is exposed about 400 m to the east in the Qf_1/Qu_1 terrace riser of Millard Creek. Thirteen meters of vertical offset would be consistent with a rate of slip >2.5 mm/yr and a north-south shortening of >2.2 mm/yr.

[27] On the Millard Canyon fan, the scarp of the SGPF does not continue northeastward beyond the modern arroyo. However, another trace of the fault runs eastward along the mountain front a couple of hundred meters to the north (Figure 6). In addition to producing a 40-m-high scarp in the Quaternary Cabezon Fm and topped by the Heights fanglomerate (Figures 6 and 9), this fault has produced meter-high scarps in small Qf_1 alluvial fans at the mountain front. Small normal faults upslope on the hanging wall block indicate that the dip of this thrust fault shallows upward in the shallow subsurface. The trace of this thrust fault disappears eastward under the very young alluvium of Deep Canyon. Here it probably connects with a southeast-striking tear fault that connects with the next thrust segment of the fault zone to the east (Figures 3a and 6).

[28] The southwestern termination of the principal trace of the SGPF on the Millard Canyon fan is near the freeway (Figure 6). Just north of the freeway, the fault zone curves toward the west and then northwestward away from the freeway. Scarps that defined this transition from southwest to northwest strikes were mapped before their destruction by construction of a large retail complex there, begun in the early 1990s. The dips of the northwest-striking structures, on the fan of Potrero Canyon are unknown. We accept the interpretation of *Matti et al.* [1985, 1992a] and *Matti and Morton* [1993] that these structures comprise a tear fault that connects thrust faults west of Potrero Canyon with those of Millard Canyon. If this is correct, their dips are probably steeply northeastward or near vertical, since only a nearly vertical tear fault could share a slip vector with the thrust fault of Millard Canyon.

3.2. Cottonwood Canyon

[29] Figure 3 shows that a major change in the style of active faulting occurs at Cottonwood Canyon. To the west, thrust faults dominate the pattern of active deformation. East of the canyon, strike-slip motions are dominant. The nature of these two systems and their interaction are critical for understanding the behavior of the San Andreas fault zone through San Gorgonio Pass.

3.2.1. East of Cottonwood Canyon

[30] The dextral-slip Coachella Valley strand of the Banning fault and the dextral-oblique Garnet Hill fault are the most prominent faults between Cottonwood and Whitewater Canyons (Figure 11). Between these two active faults is Whitewater Hill, the geomorphic manifestation of an active anticline in the Pleistocene Cabezon fanglomerate.

[31] Between Cottonwood and Whitewater Canyons, the Coachella strand of the Banning fault separates crystalline rocks from the Cabezon Fm across a deep east-west-trending fosse. The linearity of the fault trace suggests that slip on the fault is primarily dextral. Additional support for the dominance of strike-slip is the source of the Cabezon gravels; clast types indicate that the gravels derive from north of the Mission Creek fault, by way of an ancestral Whitewater River [*Allen*, 1957; *Matti et al.*, 1985, 1992a; *Matti and Morton*, 1993]. The position of Whitewater-derived Cabezon gravels at Cottonwood Canyon requires about 4 km of dextral slip (the distance from Whitewater to Cottonwood Canyons) on the Coachella Valley strand of the Banning fault, assuming that deposition occurred in front of the present Whitewater Canyon. Paleocurrent indicators led *Matti et al.* [1985, 1992a] and *Matti and Morton* [1993] to propose about 2–3 km of dextral slip here.

[32] Small dextrally offset gravel shutter ridges along the Coachella Valley strand of the Banning fault (near A on Figure 11) demonstrate that the most recent several meters of dislocation across the fault also have been right-lateral.

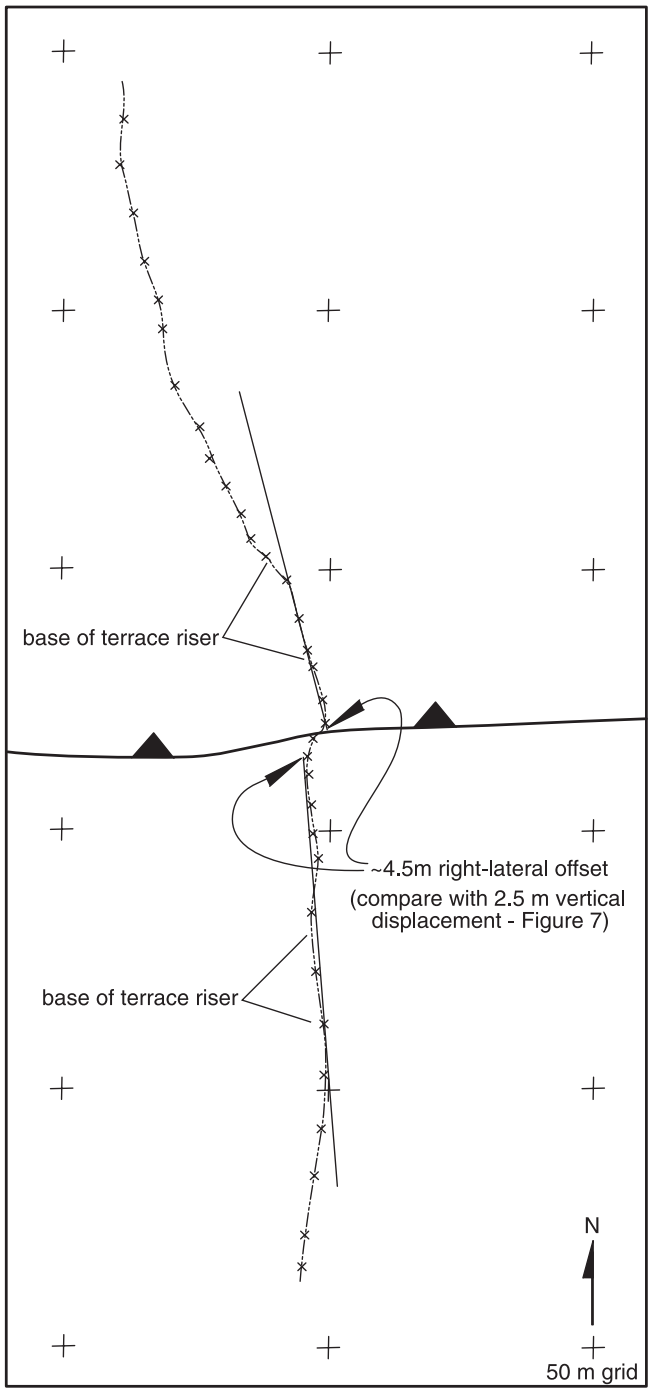

Figure 8. Map view of survey along the base of a terrace riser between Qf_2 and Qf_3 where it shows a right-lateral offset of about 4.5 m across the active segment of the Banning fault. This is about 80% greater than the vertical component (2.5 m), somewhat less than the vertical/lateral ratio of the offset of a buttress unconformity in the late Pleistocene Heights fanglomerate, exposed in the east wall of Millard Canyon (Figure 6, inset map; see text for details).

Dextral deflections of channels cut into bedrock (near B on Figure 11) also indicate a predominance of recent dextral slip. These small, young landforms near A and B also suggest that the rate of dextral slip diminishes westward along this reach of the Coachella Valley strand of the Banning fault. Contrary to expectations, the most pronounced small offsets are in rugged terrain, near A, rather than in the more gentle terrain near B. One would expect rapid erosion and burial in front of the steep, small, gravelly channels eroded into the 130-m-high gravelly escarpment at A. Less erosion and burial would be likely in the gentler terrain at B. A higher slip rate, and hence a substantially more rapid rate of creation of small tectonic landforms near A than near B, is the best explanation for this anomaly. The Coachella Valley strand of the Banning fault ends as an active strike-slip fault at Cottonwood Canyon. Although the faulted bedrock contact continues west across the canyon, the fault on the west side shows no evidence of recent activity and is a thrust fault.

[33] A depositional surface with a deep-red soil, indicative of $\geq$100,000 years of exposure, caps the fluvial Cabezon deposits of Whitewater Hill. This surface has an anticlinal shape (Figure 11). Moderate dips in the underlying deposits define this anticlinal warp as well. The deposits are more deformed than the surface, so the anticline was growing during, as well as after, deposition of the sediments, and the soil has formed on an erosional surface. A group of northwest-trending dip-slip faults cut the deposits and the old surface. Their orientation suggests that they are normal faults. The faults define a minor system of graben and horst, which are evidence for extension across the east flank of the anticline [e.g., *Yeats*, 1986]. If we assume that the surface is $\geq$100,000-years old, based on the extreme development of the capping soil, a 4-km (maximum) offset of the deposit would have accrued at an average rate of 40 mm/yr or less. This is not a very tight constraint on the slip rate of the Coachella Valley strand of the Banning fault here, but it does suggest that the rate of slip is high, on the order of centimeters rather than millimeters per year.

[34] The Garnet Hill fault bounds the southern flank of the Whitewater Hill anticline. It has two traces, one along the flank of the steep southern slope of the anticline, and another in the young alluvium farther south [*Matti et al.*, 1992a; *Matti and Morton*, 1993; *Morton et al.*, 1987]. The subtle scarp in young alluvium is only a meter or so high and its orientation, about N75°W, suggests that the scarp is the result of oblique motion on a dextral thrust fault, north over south. There is strong geomorphic evidence that slip on the other fault, at the base of the anticline, is a combination of dextral and reverse. Most of the large drainages crossed by this structure have distinct, large shutter ridges at their mouths. The stream channels deflect right-laterally around these ridges. By the Rule of V's, the trace geometry of the fault indicates a steep to moderate dip northward, under the anticline.

[35] Neither of the two traces of the Garnet Hill fault continues across the young fan deposits of Cottonwood Canyon. Thus the relationship of these faults to the active thrust faults west of the canyon is obscure.

3.2.2. West of Cottonwood Canyon

[36] Active reverse faults dominate the neotectonic landscape west of Cottonwood Canyon (Figure 11). Small scarps in young alluvium, the clearest direct evidence of the latest event or events, appear only along a short segment of the mountain front (near C in Figure 11).

[37] Elsewhere youthful scarps have presumably been either buried or eroded. However, many old alluvial surfa-

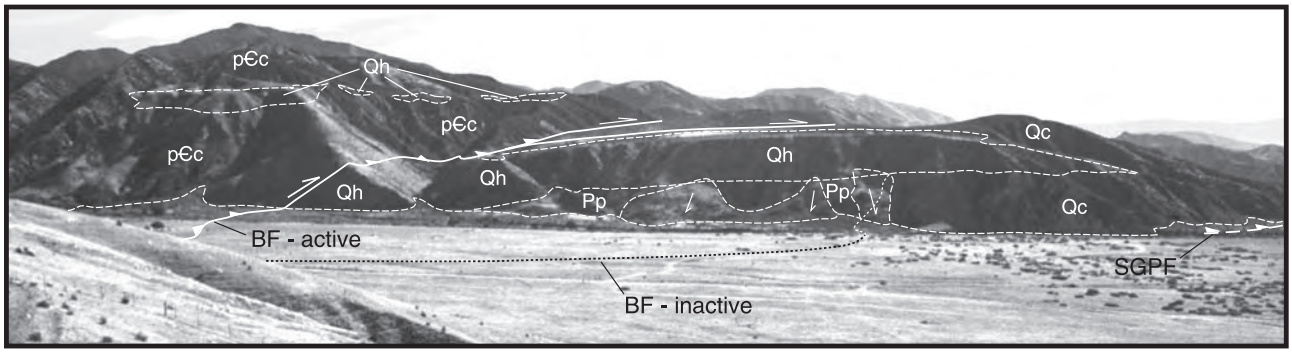

Figure 9. Tiled photographs of the east wall of Millard Canyon. An abandoned alluvial surface on the top of the late Pleistocene Heights fanglomerate (Qh) has been uplifted about 85 and 170 m across the San Gorgonio Pass and Banning faults, respectively, above the Holocene alluvial surface in the foreground (see text, Figures 6, 8, and 10). The inactive strand of the Banning fault thrusts Pliocene rocks (Pp) over the Cabezon Formation (Qc) in the middle of the photo. Rock unit symbols are as shown in Figure 6.

ces along the mountain front project well above neighboring active alluvial fans. This is clear evidence for uplift on faults at and near the mountain front. For example, a few hundred meters south of the mountain front (near D in Figure 11) a broad active channel separates an old alluvial surface into two remnant terraces. Young alluvium laps onto both remnants on their northern edges and onto the eastern flank of the eastern remnant. A stream has eroded the western flank of the western remnant. The southeastern edges of both terrace remnants are also eroded, but that erosion is not due to stream erosion. Uplift of the terraces along a northeast-southwest-striking fault is a more viable interpretation. The orientation of this scarp supports the interpretation that the causative fault is a reverse fault that dips northwest, toward the mountains.

[38] Other alluvial terraces along the mountain front between Stubbe and Cottonwood Canyons belie the presence of another thrust fault, structurally above the one just described (between E and F on Figure 11) [*Morton et al.*, 1987; *Sieh and Matti*, 1992; *Matti and Morton*, 1993]. The trace of this fault is buried beneath young alluvium along most of its length; but it must follow the irregular shape of the mountain front, because the triangular facets of the mountain front cannot be due to stream erosion parallel to the mountain front. For the same reason, uplift of the lobate, alluvial terrace west of the mouth of Stubbe Canyon (Figures 3a and 11) must also be related to slip on an arcuate active thrust fault that circumscribes that lobe of the mountain front.

[39] A large rotational landslide obscures the geologic relationships of the slopes immediately west of Cottonwood Canyon (Figures 11 and 12) [*Morton et al.*, 1987]. The headscarp and lateral margins of this slide are readily apparent and leave no doubt that the feature is of nontectonic origin. A small sector on the western flank of the slide slumped again in 1993. The high degree of preservation of the landslide suggests that it is no more than a few thousand years old. The toe of the landslide partially overrides a paleochannel cut into crystalline bedrock and old alluvium (near G on Figure 11, and Figure 12). This

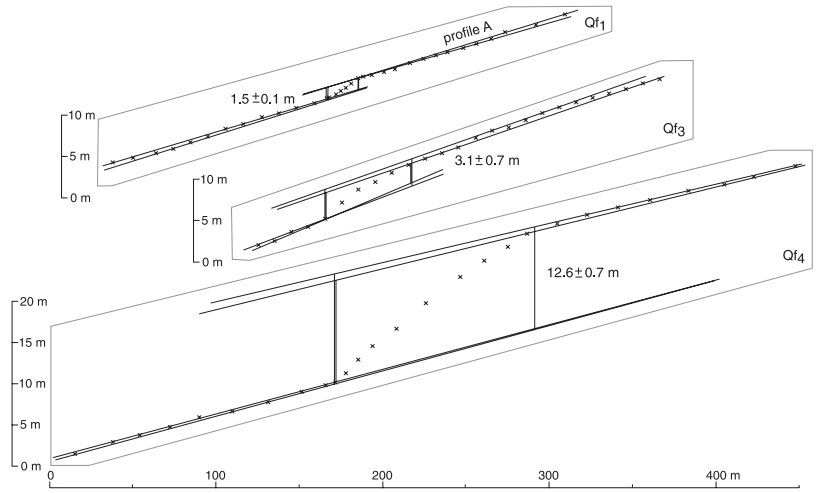

Figure 10. Cross-sectional view of surveyed profiles across the SGPF in Millard Canyon (see Figure 6 for locations of profiles). Vertical offsets were calculated as described for Figure 7. See text for discussion of slip-rate estimates based on these offsets.

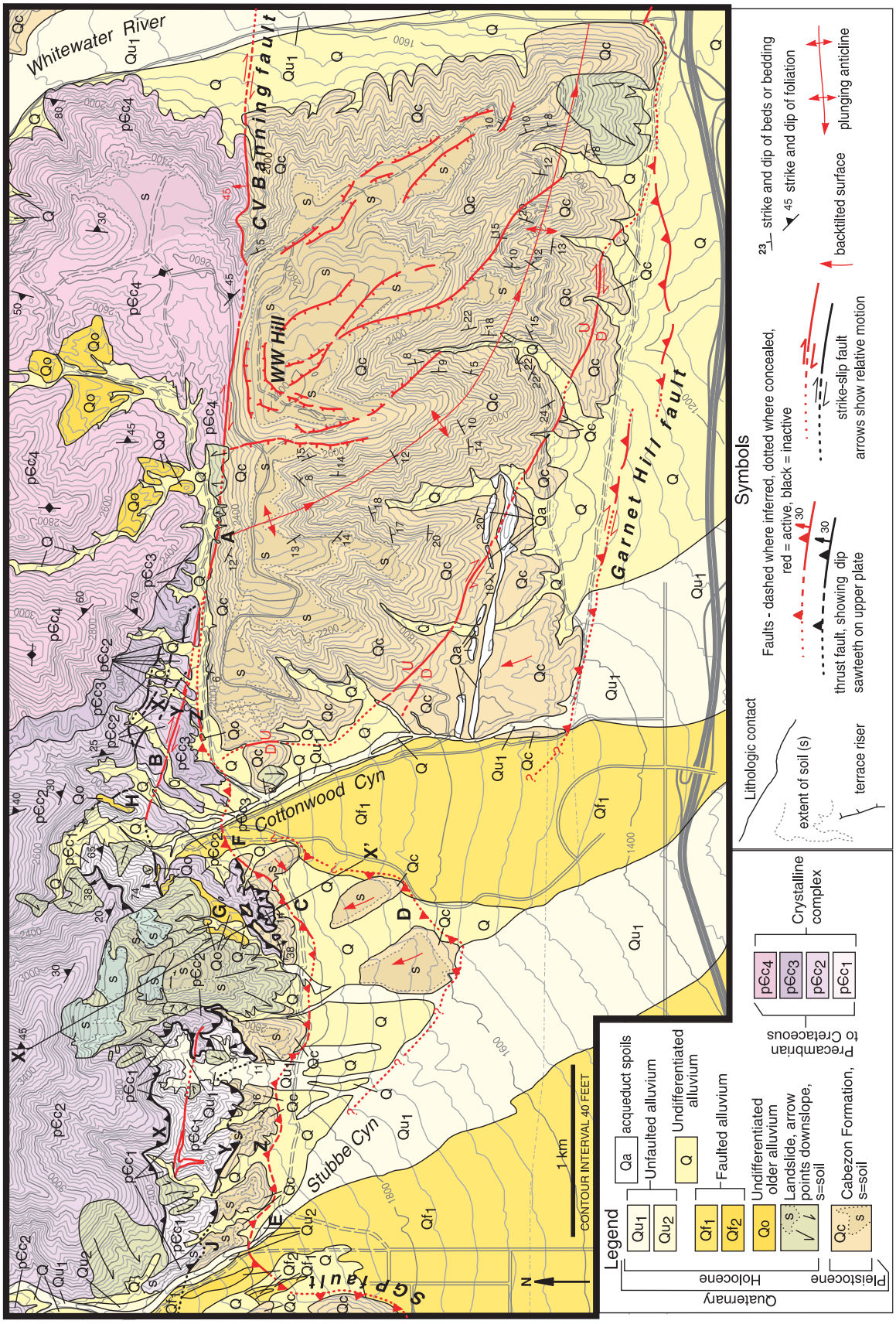

Figure 11. Geologic map of the Cottonwood Canyon area [portions modified from *Matti et al.*, 1992a; *Sieh and Matti*, 1992; *Matti and Morton*, 1993; *Morton et al.*, 1987; R. Wolf, unpublished mapping] shows the convergence of predominantly right-lateral faults (east of the canyon) with predominantly reverse-slip active faults (west of the canyon). See Figure 3a for the location of the map. Figure 12 is taken along line of cross section X-X'.

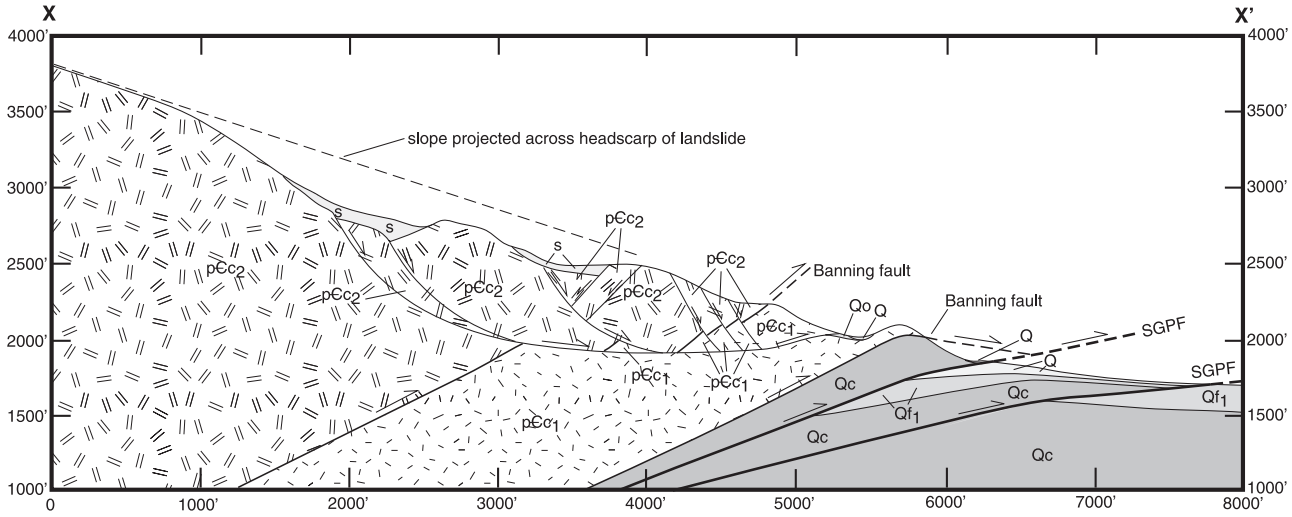

Figure 12. Geologic cross section along line X-X' (location shown in Figure 11). Note the two active fault strands of the San Gorgonio Pass fault (SGPF), dipping shallowly to the north. Strands of the Banning fault thrust Cretaceous to Precambrian crystalline rocks (pCc_1 and pCc_2) over late Pleistocene Cabezon Formation (Qc) but are considered inactive. The landslide in the hanging wall shows a clear headscarp and lateral margins.

relationship is clear at the eastern end of the buried channel, in an exposure on the west wall of Cottonwood Canyon. This channel appears to have served as a conduit for Cottonwood creek prior to its burial by the slide and prior to a few tens of meters of incision by Cottonwood creek. The outlet of the buried channel (at the mountain front) aligns with the broad channel that bisects the old alluvial deposits at D (J. Treiman, oral communication, 1992). These channels were probably contiguous when active, but uplift of the mountain front has led to deposition of younger alluvium between them, completely burying the old channel immediately downstream from the mountain front.

[40] Numerous older, inactive thrust faults crop out north of the active mountain front [*Morton et al.*, 1987; *Sieh and Matti*, 1992; *Matti and Morton*, 1993]. We show the obvious ones (those mappable by virtue of their juxtaposition of crystalline basement units over one another and over older alluvial deposits) (Figures 11 and 12). The lack of geomorphic expression indicates that none of these shallow-dipping structures is active. In addition, unbroken old alluvium or old surfaces bury some, or fensters have been cut through them. All but the northernmost of these inactive faults override old alluvium and alluvial surfaces and have thus been active in the late Pleistocene. Their contiguity with the Coachella Valley strand of the Banning fault at Cottonwood Canyon suggests that they were active when dextral slip on the Coachella Valley strand of the Banning fault transformed into thrust faulting at Cottonwood Canyon.

3.2.3. Connections

[41] Geologic relationships near the mouth of Cottonwood Canyon place important constraints on the interactions between faults west and east of the canyon. An interpretation of these relationships must precede our discussion of a tectonic concept for the region.

[42] The Coachella Valley strand of the Banning fault splays into three traces as it approaches Cottonwood Canyon from the east (X, Y, and Z on Figure 11). The two northernmost traces (X and Y on Figure 11) connect across the canyon with steep to gently dipping inactive strands of the Banning fault. The northernmost inactive strand is buried by the large landslide on the west wall of the canyon and by a thin alluvial gravel high on the east wall (H on Figure 11). It emerges west of the landslide as an inactive thrust fault within crystalline basement rocks. The southernmost inactive fault connects across Cottonwood Canyon with the strand of the Coachella Valley strand that has the clearest geomorphic evidence for dextral slip (B on Figure 11). West of the large landslide, this thrust fault places crystalline basement rocks over an alluvial terrace remnant. On the east side of Stubbe Canyon, this fault is overlain by a younger fluvial terrace remnant and soil (J on Figure 11). The current inactivity of both of these thrust faults is consistent with the observation that dextral slip on the Coachella Valley strand of the Banning fault dies out westward as it approaches Cottonwood Canyon [*Allen*, 1957; *Matti et al.*, 1985, 1992a]. The subtle geomorphic evidence for dextral slip on the Coachella Valley strand just east of Cottonwood Canyon (A on Figure 11) is consistent with activity on the thrust fault in the not too distant past, say 10^4–10^5 years ago.

[43] The presence of Whitewater Hill anticline, between the Garnet Hill fault and the Coachella Valley strand of the Banning fault, implies a transfer of dextral slip from the latter fault onto the former [*Matti et al.*, 1985, 1992a]. Geomorphic evidence for westward diminishment of dextral slip on the Coachella Valley strand is clear. This diminishment may be translated into shortening across the anticline and increased slip westward on the Garnet Hill system. In addition, dextral slip may be translated to the north via transtension onto the oblique dextral-normal Cox Ranch

fault zone. Regardless of the details of this transfer, all of the slip on the Coachella Valley segment ceases by Cottonwood Canyon; and so, these other structures must absorb the slip [*Matti et al.*, 1985, 1992a].

[44] The geomorphic expression of the Garnet Hill fault shows no sign of diminishing as it approaches Cottonwood Canyon from the east. The geomorphic expression of the active thrust faults at and in front of the range shows no signs of diminishing as they approach the canyon mouth from the west. We suspect, therefore, that these two fault zones are contiguous beneath the young alluvium of Cottonwood Canyon. Much of the dextral slip on the Garnet Hill fault could be transformed into reverse slip on the thrust faults of the SGPF zone, as *Matti et al.* [1985, 1992a] originally proposed.

4. Regional Folds and Blocks

[45] Flexure of fault-bounded crustal strips accommodates a significant component of the strain in the San Gorgonio Pass stepover region [*Dibblee*, 1975]. The regional warping has northwest-trending axes in the southern San Bernardino Mountains and a west-trending axis in the northern San Jacinto Mountains (Figure 2b). Evidence of regional scale flexures includes anomalously high topography, gross geomorphology, deformed late Quaternary sediments, and (U-Th)/He thermochronologic data. Below, we consider each of several large blocks, separately.

4.1. Morongo Block

[46] The Morongo block is characterized by a central topographic high at Kitching Peak, which rises about 1–1.5 km above low-lying areas to the west and east (Figure 2b). South flowing drainages of the upper San Gorgonio and Whitewater Rivers deflect toward the west and east, respectively, around this topographic high. Kitching Peak is also surrounded by outliers and outcrop belts of late Pleistocene deposits (Figure 3a). Miocene to middle Pliocene strata to the east of Whitewater River dip 20°E to NE on average. These observations can be explained by a northwest-trending arch of late Quaternary age with limbs gently plunging to the east and west from the central topographic high of the Morongo block. (U-Th)/He samples are being analyzed to help constrain the geometry of this structure [*Spotila et al.*, 2001].

4.2. Yucaipa Ridge

[47] Yucaipa Ridge is a rugged, elongate ridge bounded by the San Bernardino strand of the San Andreas fault and the Mill Creek fault. The ridgeline elevation increases steadily from ~1.5 to 3 km toward the east-southeast (Figure 2b) [*Spotila et al.*, 1998]. A ridgeline profile is therefore similar to the profile of the western flank of the Morongo block. Apatite (U-Th)/He cooling ages indicate that the Yucaipa Ridge block experienced >3 km of Quaternary denudation about 1.5 myr ago [*Spotila et al.*, 1998, 2001]. We suggest that more recent uplift, westward tilting, and erosion may have attended broad uplift of the region.

4.3. San Gorgonio Mountain Block

[48] The San Gorgonio Mountain block; [*Dibblee*, 1975, 1982; *Sadler and Reeder*, 1983] is also characterized by a central topographic high of ~1–1.5 km higher than regions to the west and east (Figure 2b). Apatite (U-Th)/He cooling ages obtained from the western flank of the block suggest that post-Miocene ~5° westward and ~10° northward tilts have occurred [*Spotila et al.*, 1998]. This tilt closely parallels the topographic gradient of the western flank of San Gorgonio Mountain. Though no cooling ages have been obtained from the eastern flank, we suspect that cooling ages will show eastward and northward tilting. Northward tilt of the block is also shown by ~25° north dips of Mio-Pliocene Santa Ana sandstone beds at Barton Flats [*Dibblee*, 1964; *Sadler et al.*, 1993]. The San Gorgonio Mountain block therefore appears to be a broad northwest-southeast-plunging arch.

4.4. San Jacinto Mountains Block

[49] The northern end of the San Jacinto Mountains block exhibits a topographic bulge centered on San Jacinto Peak. Relief to the south and west is about 1 km and to the north and east is over 3 km. Southeast-northwest-trending profiles across the arch define a west-plunging topographic arch (Figure 2b). (U-Th)/He apatite cooling ages [*Wolf et al.*, 1997] loosely define thermochrons that show flexure that mimics the broad topographic arch (see discussion below). Hornblende barometry and (U-Th)/He apatite cooling ages also document a modest westward tilt about a N-S tilt-axis of the San Jacinto block, roughly parallel to the topographic profile [*Ague and Brandon*, 1992; *Wolf et al.*, 1997]. The age of this structure, constrained by apatite cooling, is post-40 Ma, but may be quite young.

5. Relevant Observations of Seismicity

[50] Recorded seismicity in the region of the Pass is important for interpreting the neotectonic behavior of the San Andreas fault system there. Rather than relying on structural modeling to extrapolate surface traces of active faults farther into the crust, we use crustal seismicity as a guide. In this section, we present relevant information about the depth of seismicity and we summarize previous work on the source parameters of small to moderate earthquakes.

5.1. Base of Seismicity

[51] The pattern of crustal seismicity in this region plays a crucial role in our interpretation of its earthquake geology. A key observation is that maximum hypocentral depths of small earthquakes beneath San Gorgonio Pass and the southern San Bernardino Mountains are anomalously deep. Whereas most of southern California experiences maximum focal depths between 10 and 15 km, this region has hypocentral depths as great as 20 km.

[52] The geographic pattern of the base of seismicity must relate to the present-day tectonics of the region. *Magistrale and Sanders* [1996] demonstrated that the deepest hypocenters cluster beneath the stepover of the San Andreas fault zone near San Gorgonio Pass. They also showed that the base of seismicity drops precipitously from 13 km or so on the north, to 20 km on the south along an east-west plane beneath the fault zone. They argued that this abrupt drop represents a sharp juxtaposition of the brittle-ductile transition for feldspar-dominated rocks of the Peninsular ranges, south of the abrupt drop, against the transition for quartz-

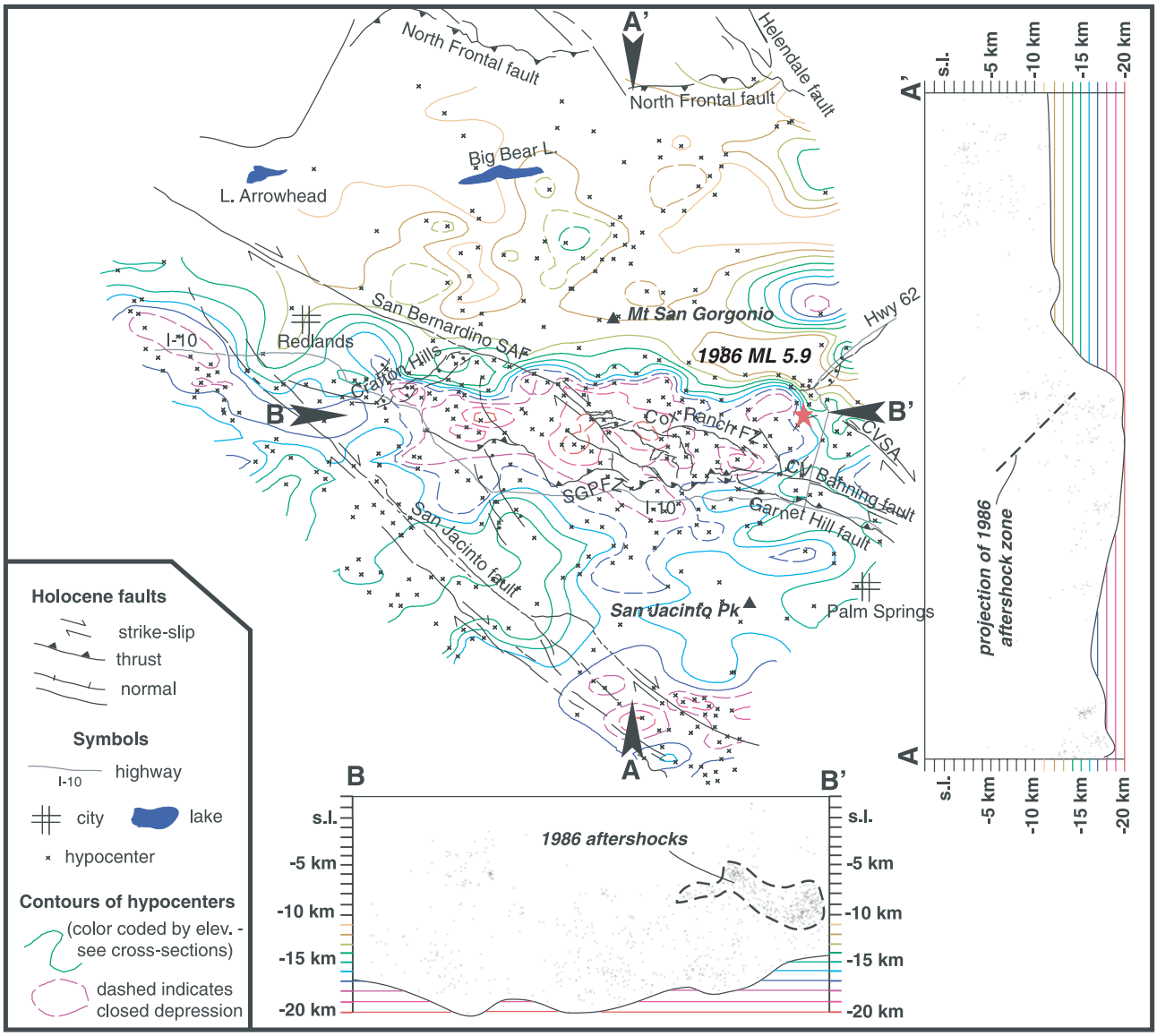

Figure 13. Contours on the base of seismicity in the SGP region show a distinct east-west-trending vertical step, 6–7 km high. The deepest hypocenters, one selected for each 3–5 km^2 area, are contoured at a 1-km interval. Hypocenters were supplied by Magistrale for the years 1981–1993. The seismicity step separates regions of anomalously deep and shallow limits of seismicity, to the south and north, respectively. Vertical cross sections A-A' and B-B' show the base of seismicity and hypocenters taken from a 5-km-wide vertical slice and projected onto the plane of cross section. The 1986 North Palm Springs aftershock sequence [*Hartzell*, 1989; *Nicholson*, 1996] intersects B-B' in a nearly horizontal plane. We use the 1986 rupture plane, as illuminated by aftershocks, to carry the San Gorgonio Pass-Garnet Hill fault system to depth (see text for further details). The along strike projection of this rupture plane is shown in A-A'.

dominated rocks of the San Bernardino Mountains, to the north. We argue below that this is not the primary reason for the drop. But first, let us describe the geometry of the base of seismicity in more detail than did *Magistrale and Sanders* [1996] and explain its geologic associations.

[53] Figure 13 is a map of the base of seismicity with the traces of active faults superimposed. We used a catalog of earthquakes supplied by Magistrale for the years 1981–1993 from the work of *Magistrale and Sanders* [1996]. Cross section A-A' shows the change in-depth of seismicity along a vertical plane, 5-km wide, perpendicular to the east-west step. This shows that the step in seismicity is about 5–8 km high. It also shows that the southern flank of the trough formed by the base of the seismicity dips very gently northward from about San Jacinto Peak. Cross section B-B' shows the change in-depth along a plane parallel to and within the trough of deepest seismicity. Comparison of the geographic extent of the trough with topography (Figure 2) shows that the trough is precisely coincident with the eastern and western flanks of the southern San Bernardino

Mountains. Furthermore, the dimensions of the trough match the dimensions of the hanging wall block of the SGPF (Figure 13). This suggests a common cause of the seismicity trough, the topography, and active faulting in San Gorgonio Pass. Another fundamental observation of *Magistrale and Sanders* [1996] is clear from the map: the San Bernardino strand of the San Andreas fault does not appear to offset the seismicity step.

5.2. Focal Mechanisms of Background Seismicity

[54] The focal mechanisms of background earthquakes within the region of deep crustal seismicity also must bear on the active tectonics of the region. *Nicholson et al.* [1986] and *Seeber and Armbruster* [1995] analyzed hundreds of events beneath the San Andreas fault zone here. *Nicholson et al.* [1986] draw a distinction between shallow and deep seismicity; above about 10 km, oblique left slip in combination with both normal and reverse faulting predominates, and below 10 km strike-slip and less common low angle thrust faulting predominates. *Nicholson et al.* [1986] attributes the change in microearthquake focal mechanism with depth to the presence of a regional detachment [also see *Hadley and Kanamori*, 1977]; a set of small, upper crustal blocks currently rotating under a regional right-lateral shear system decoupled from a wedge-shaped region of the lower crust experiencing pervasive north-south shortening and east-west extension. *Seeber and Armbruster* [1995] envision shortening accommodated by north-dipping thrust faults, primarily the SGPF in the upper crust and a San Gorgonio Pass detachment at depth; extension is accommodated by dextral strike slip on the San Andreas, a throughgoing feature beneath the SGPF. A scarcity of hypocenters above 5-km depth makes connecting faults at depth with surface faults problematic. Furthermore, both studies caution that the great majority of microearthquakes occur off the primary structures, and that the pattern indicated from microseismicity, collected over a relatively short time period (10–20 year), might not characterize the primary active tectonic features of the Pass region.

5.3. The 1986 North Palm Springs Earthquake

[55] Studies of the M_L5.9 North Palm Springs earthquake and aftershock sequence show another critical relationship between the seismicity step and certain active faults of the stepover. The focal mechanism and aftershock zone determined by *Jones et al.* [1986] show that the source of the earthquake was a 50°-NE-dipping, N60°W-striking fault. The short-period mechanism shows that slip was purely right-lateral, but an analysis of long-period waves [*Hartzell*, 1989] indicates that slip during most of the rupture was highly oblique, with significant components of reverse, as well as dextral slip. The ratio of dextral to reverse slip was between 1:1 and 2:1.

[56] Regardless of the slip vector, the fault plane projects updip to the trace of either the Coachella Valley segment of the Banning fault or the trace of the Garnet Hill fault [*Jones et al.*, 1986]. The oblique-slip motion of the 1986 rupture is compatible with the sense of slip of the Garnet Hill fault at the surface, with the uplifted Pleistocene gravels of east and west Whitewater Hill (Figure 3b) an indication of the dip-slip component in its hanging wall. It is inconsistent with the geometry and sense of slip on the Coachella Valley strand of the Banning fault at the surface, which is subvertical east of Whitewater Canyon [*Allen*, 1957] and nearly pure strike slip. We interpret the more steeply dipping Coachella Valley strand to reside in the hanging wall of a more gently dipping fault whose surface expression is the Garnet Hill fault. We therefore conclude that the 1986 earthquake ruptured a single fault plane that bifurcates into the Garnet Hill and Coachella Valley strand of the Banning fault above about 5-km depth, the upper limit of the aftershocks.

5.4. The 1948 Desert Hot Springs Earthquake

[57] Another important earthquake for our analysis is the M_W6.0 Desert Hot Springs earthquake. *Nicholson*'s [1996] seismographic comparison of the 1948 and 1986 earthquakes shows that the earlier earthquake involved rupture of a fault plane immediately southeast of the 1986 rupture. The strike of the plane is slightly more northerly than the 1986 rupture (N55°W), the dip is slightly steeper (60°–70°), and the slip vector has a much smaller component of reverse slip (a rake of only bout 10°). These parameters are consistent with rupture of either the Coachella strand of the Banning fault or the Garnet Hill fault, southeast of the 1986 rupture. Along this reach, even the Garnet Hill fault displays only local geomorphic evidence of vertical slip, associated with small en echelon stepovers inferred for the fault trace.

6. Kinematic Concept

[58] We are now prepared to attempt a synthesis of the data we have presented above. Our analysis of active faults and folds, augmented by seismicity, provides a basis for constructing a three-dimensional model of active deformation. Later, we discuss the impact of our three-dimensional crustal model on plausible sources for future and past large earthquakes in the region.

[59] Recent explanations of the active tectonics of the San Andreas fault zone in the region of San Gorgonio Pass have differed substantially. Two of these recent proposals involve the concealment of a more-or-less straight and contiguous San Andreas fault zone through the region. *Rasmussen and Reeder* [1986] suggest, on the basis of geomorphologic evidence, that the San Andreas fault continues as a simple strike-slip fault beneath the region, obscured at the surface by a very large landslide complex (Figure 14a). *Seeber and Armbruster* [1995] believe that the SGPF is an active thrust fault, but from the alignment of about 20 strike-slip focal mechanisms, conclude that it conceals the principal active structure, which is a simple, throughgoing strike-slip fault at depth (Figure 14b). A third interpretation, synthesized by *Matti et al.* [1985, 1992a], *Matti and Morton* [1993], and *Morton and Matti* [1993], and supported by *Magistrale and Sanders* [1996], envisions a left-stepping zone of convergence with a discontinuous system of strike-slip and thrust faults that transfers dextral slip through the region. Our mapping and analysis refutes the first two models and substantiates the third. We propose the geometry and senses of slip illustrated in Figure 14c.

6.1. Landslide Hypothesis

[60] The landslide hypothesis [*Rasmussen and Reeder*, 1986] is not consistent with the geometry and sense of slip

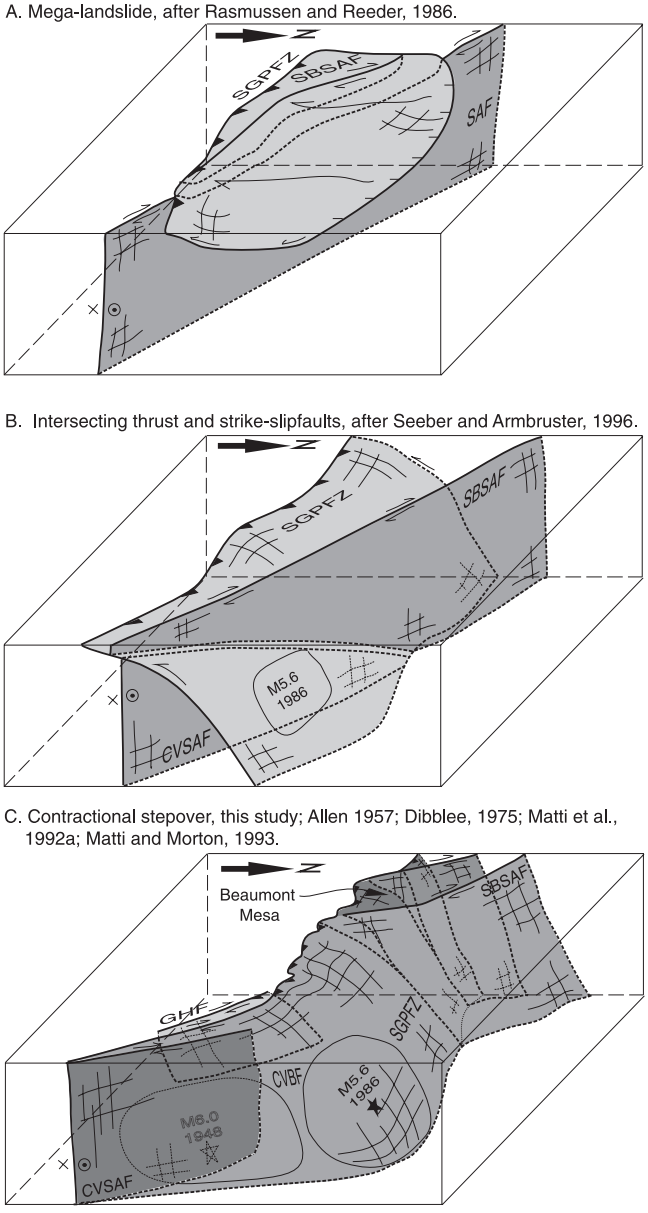

Figure 14. Three block diagrams illustrate three alternative kinematic models for the active faults of the San Gorgonio Pass region. (a) In this mega-landslide model [*Rasmussen and Reeder*, 1986] a large landslide overrides and obscures the vertical plane of the San Andreas fault. (b) In this thrust-flap model [Figure 3c of *Seeber and Armbruster*, 1995] a south-vergent thrust fault offsets the vertical, strike-slip plane of the San Andreas fault. (c) In the fault-bend-fold model [modified from *Allen*, 1957; *Dibblee*, 1968, 1975, 1982; *Matti et al.*, 1985, 1992a; *Matti and Morton*, 1993], which we advocate, vertical to moderately dipping strike-slip planes cut the hanging wall block of the SGP thrust fault on the west and approach the thrust fault on the east. Only the latter model fits the data we have presented in this paper. Dashed lines indicate features in the background. Abbreviations include SGPFZ, San Gorgonio Pass fault zone; SBSAF, San Bernardino strand, San Andreas fault; SAF, San Andreas fault; CVSAF, Coachella strand, San Andreas fault; and CVBF, Coachella Valley strand, San Andreas fault.

on the active features of the region. One of its serious deficiencies is the lack of a credible headscarp in the southern San Bernardino Mountains. The most obvious candidate for a headscarp would be the Cox Ranch fault zone, since this structure does have a significant component of normal dip slip and traverses the entire stepover region. But the en echelon geometry of the Cox Ranch fault zone and its clear dextral component of motion are inconsistent with a landslide origin. Slip on the western third of the Cox Ranch fault zone would, for example, need to be left-lateral if it were the headscarp of a large landslide that had the dextral-slip faults in Potrero Canyon as its western margin and the San Gorgonio Pass thrust as its toe (Figure 3a). Furthermore, this portion of the SGPF west of Potrero Canyon has no extensional structures to the north that would support the hypothesis that it is the toe of a large landslide (Figure 2). A similar lack of candidate headscarps (and the large component of dextral slip) leads to rejection of the Garnet Hill fault zone as the toe of a massive landslide. Although it is true that the mountainous region north of the Pass is rife with landslides (Figure 3a), none of these is large enough to claim the thrust faults as their toe.

6.2. Thrust-Flap Hypothesis

[61] *Seeber and Armbruster*'s [1995] hypothesis is based upon the existence of about 20 hypocenters with strike-slip mechanisms beneath the region, at depths of 11–22 km. On the west, these hypocenters are coincident with the 5–8 km high step in the base of seismicity; on the east, they are several kilometers south of the step. These hypocenters align approximately N70°W between the San Bernardino strand of the San Andreas fault and the Coachella Valley strand of the Banning fault, though in detail this trend deviates from the N45°W trend of the San Andreas strand at its southern extent in Potrero Canyon (Figure 3a).

[62] The principal flaw in a thrust-flap hypothesis is that it predicts the existence of decapitated remains of steeply dipping strands of the San Andreas fault within the thrust flap (as illustrated in Figure 14b). Our mapping precludes the existence of structures that could be interpreted as such. The only candidates are the dormant strands of the Banning fault (Figures 2 and 3a), a set of thrust faults whose geometry and kinematics identifies them as precursors to the SGPF, not the San Andreas fault. This does not mean that a handful of strike-slip mechanisms do not form an east-west alignment beneath the region. But the aligned events do not appear to illuminate a major strike-slip structure there. The use of just a handful of selected small earthquakes to characterize a major neotectonic element of the San Gorgonio stepover, the 20 hypocenters constitute a small fraction of the strike-slip mechanisms beneath the region [Figure 4 of *Seeber and Armbruster*, 1995], is analogous to using a handful of bricks in the wall of a building to characterize the wall. In this case, we find no reason to believe that these few bricks are representative of a major active structure.

6.3. Transpressional Stepover Hypothesis

[63] *Allen* [1957] proposed, as one of five possible models, that the San Bernardino and Coachella Valley strands of the San Andreas fault do not connect but transfer slip via thrust faulting in the San Gorgonio Pass region.

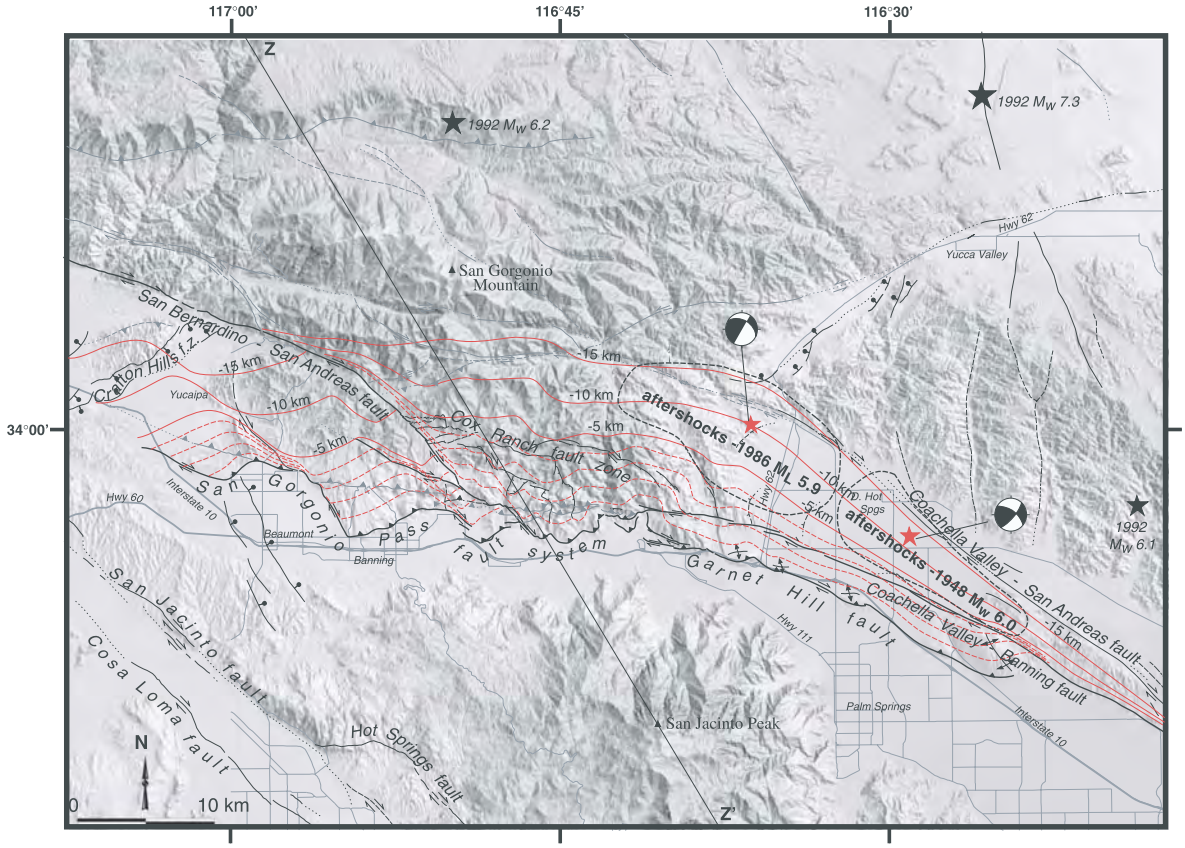

Figure 15. Structural contour map of the primary fault systems of the San Gorgonio Pass region. These structural contours on the active elements of the San Andreas and San Gorgonio Pass fault zones are constrained by geologic mapping, regional seismicity, and the aftershocks of the 1986 M_L5.9 North Palm Springs and the M_w6.0 1948 Desert Hot Springs earthquakes (dashed outlines). In this interpretation, the San Bernardino strand of the fault is a tear fault in the hanging wall block of the San Gorgonio Pass fault system. The moderately dipping Garnet Hill and more steeply dipping Coachella Valley Banning fault strands merge at depth and merge with the San Gorgonio Pass fault system from the east.

Dibblee [1968, 1975, 1982] modified another model of *Allen* [1957] describing how the San Bernardino strand, Coachella Valley strand, and Banning fault once formed a throughgoing trace within the Pass region that was subsequently deflected into a sharp transpressive bend. *Matti et al.* [1985, 1992a] and *Matti and Morton* [1993] cite evidence that indicates slip dies out on the San Bernardino and Coachella Valley strands as they approach the San Gorgonio Pass region from the northwest and southeast, respectively. They view the San Gorgonio Pass region as a structural knot whereby slip is transferred around the knot via the Coachella Valley Banning fault, SGPF system, Crafton Hills fault system, and San Jacinto faults.

[64] Together, geologic and seismographic data support an interpretation whereby the dominant structure of the Pass region is a wide, complex, transcrustal oblique-slip fault system, bounded on the south by the San Gorgonio Pass-Garnet Hill fault zones. We propose that slip on these, the other active structures of the Pass region (Figures 2 and 15), and perhaps, significant rotations between them, account for about half, if not more, of the 20–25 mm/yr of dextral slip measured across the San Andreas fault zone outside of the stepover region [*Weldon and Sieh*, 1985; *Harden and Matti*, 1989; *van der Woerd et al.*, 2001].

[65] A structural contour map of the southern boundary of these fault systems (Figure 15) illustrates in three dimensions our concept of the principal, active crustal structure of the San Gorgonio Pass region and the data upon which it is based. We adopt the time-space model of *Matti and Morton* [1993] and infer that the geometry for active structures shown in Figure 15 has evolved in the last 125,000 years or so. The geologic architecture of the region centers on the north-dipping, dextral-reverse San Gorgonio Pass-Garnet Hill fault zone. We show the Garnet Hill fault and the Coachella Valley, Banning fault merging at a depth to form a single fault plane below about 5 km. We believe that the aftershock zones from 1986 and 1948, shown as patches on this fault at depths between about 5 and 15 km, illuminate this ''master fault'' at depth that bends to the west to become the SGPF zone. Figure 15 shows the San Bernardino strand of the San Andreas fault as a large tear fault in its the hanging wall. The SGPF zone continues to the west, transferring a component of slip to the northern San Jacinto fault and back to the San Bernardino strand via the Crafton Hills fault zone [see Figure 6 of *Matti et al.*, 1992a]. The San Gorgonio Pass-Garnet Hill fault zone therefore is the locus of south-under-north thrusting created by the oblique collision of the northeastern corner of the Peninsular Ranges

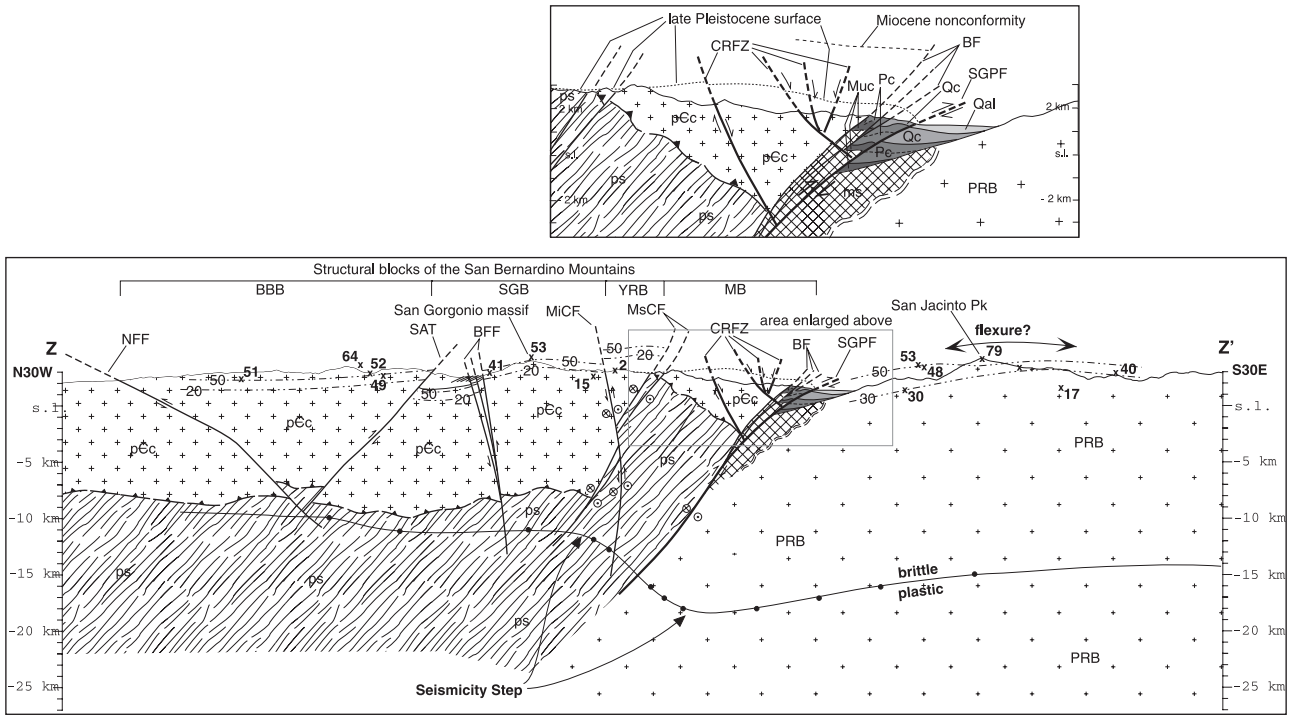

Figure 16. Interpretive regional cross section that is consistent with surface geologic observations and regional seismicity. See Figure 15 for line of cross section. Faults are projected downward based on surface dips, taken from *Allen* [1957], *Dibblee* [1982], *Matti et al.* [1985], and this study. Basement units are juxtaposed by strike slip on the Mission Creek fault and the ancestral Banning-San Gabriel fault [*Matti and Morton*, 1993]. The Pelona schist occupies the deepest structural level in the eastern Transverse Ranges suggesting that it comprises the deep crust beneath the granitic upper crust of the San Bernardino Mountains [*Matti and Morton*, 1993]. Exposures of the Pelona schist to the north of Burro Flats beneath the Vincent thrust (Figure 3a) indicate that it comprises much of the crust between the San Gorgonio Pass and Wilson Creek faults. The Banning and San Gorgonio Pass faults represent an in-sequence fold and thrust belt that has accommodated Quaternary south-under-north convergence between the San Bernardino and San Jacinto Mountains. Dashed-dotted parallel lines are the 20 and 50 Ma and the 30 and 50 Ma helium isochrons interpreted for the San Bernardino Mountains [*Spotila et al.*, 1998] and the San Jacinto Mountains [*Wolf et al.*, 1997]. Helium data, bold 'x' and number, projected perpendicular to cross sections. The He isochrons are elevated and depressed to the north and south of the San Gorgonio Pass fault, consistent with south-under-north convergence and associated regional warping (Figure 2a). Abbreviations of structural blocks as shown in Figure 2b; rock unit abbreviation as in Figure 3. Fault abbreviations: NFF, North Frontal fault; SAT, Santa Ana thrust; BFF, Barton Flats fault; MiCF, Mill Creek fault; MsCF, Mission Creek fault; CRFZ, Cox Ranch fault zone; BF, Banning fault; SGPFZ, San Gorgonio Pass fault.

(San Jacinto Mountains) with the eastern Transverse Ranges (San Bernardino Mountains). Below, we explain how we constructed this structure contour map.

6.4. Extrapolation of the 1986 Rupture Plane

[66] We have argued that the characteristics of the 1986 rupture are consistent with the Garnet Hill fault being the source of the 1986 North Palm Springs earthquake. The geographic coincidence of the 1986 fault rupture and the step in deepest seismicity (A-A', Figure 13) suggest to us that the Garnet Hill fault is responsible for the step in seismicity. Since the Garnet Hill fault appears to transform into the San Gorgonio Pass fault at Cottonwood Canyon, slip on the latter fault may also be responsible for the step in seismicity. Using the rupture plane defined by the 1986 main shock and aftershocks as a starting point, we have drawn structural contours for the entire San Gorgonio Pass-Garnet Hill fault system so that the fault planes extend downward from the surface to the middle of the step in seismicity (15-km depth) (Figure 15).

[67] The contours updip from the 1986 rupture represent the fault plane between the 1986 rupture plane and the surface trace of the Garnet Hill fault. Southeast of the 1986 rupture plane, the closer spacing of the contours and their more southerly trend are consistent with *Nicholson*'s [1996] mechanism for the 1948 earthquake and with the surface strike of the Garnet Hill fault. (To keep the figure uncluttered, contours of the Coachella Valley strand of the Banning fault do not appear in Figure 15. We envision this steeper strike-slip fault wholly within the hanging wall block of the Garnet Hill fault (Figure 14c).)

[68] Farther west, between the surface trace of SGPF zone and the seismicity step, the contours show a fault plane that steepens gradually from about 30° dips near the surface to

Table 1. Plausible Moment Magnitudes for Major Active Faults and Fault Systems

Name	Surface Area, km^2	d,[a] m	Moment,[b] Nm	M_W
Cox Ranch fault zone[c]	20 × 7 = 140	2.0	8.4×10^{18}	6.6
Coachella Valley Banning-Garnet Hill faults[d]	CVB, 45 × 17 = 765; GHF, 30 × 5 = 150; total area = 915	3.5	9.6×10^{19}	7.3
San Gorgonio Pass fault[e]	55 × 22 = 1210	4.0	1.5×10^{20}	7.4
San Bernardino SAF[f]	80 × 15 = 1200	4.0	1.4×10^{20}	7.4
Coachella Valley SAF[g]	115 × 15 = 1725	4.0	2.1×10^{20}	7.5
SGP-GH-CVB	total area = 2125	4.5	2.9×10^{20}	7.6
CVSAF-CVBF-GHF	total area = 2640	5.0	4.0×10^{20}	7.7
All faults	total area = 5190	5.0	9.3×10^{20}	7.9

[a]Average surface displacement.
[b]We assume a shear modulus of 3×10^{10} Nm^{-2}.
[c]This includes all sections of the fault system.
[d]This assumes that the western end of the CVB is at Cottonwood Canyon and that the CVB and GH faults merge at a depth of about 5 km.
[e]This assumes the active portion extends from Calimesa to Cottonwood Canyon.
[f]This includes the active portion of the Gandy Ranch and Banning faults, near Millard Canyon.
[g]This assumes the active portion extends from the Salton Sea to Highway 62.

about 60° dips at about 15 km. This convex-upward geometry in the fault plane is consistent with minor extension within the hanging wall block along the Cox Ranch fault zone (Figure 2a), and with the broad fold in the Morongo block (Figure 2b). First-order irregularities in the strike of the seismicity step (Figure 13) suggest the existence of a few bends in the plane of the SGPF at the seismicity step.

[69] The biggest challenge in creating a structure contour map of the fault zone is the sharp transition from oblique slip to thrust faulting that *Morton et al.* [1987], *Matti and Morton* [1993], and we have mapped at Cottonwood Canyon. To be consistent with this markedly abrupt change in surficial expression of faulting, we have chosen to bend the structure contours sharply at Cottonwood Canyon. We have drawn the down-plunge projection of this bend as a broad warp pointing toward the aftershock region of the 1986 earthquake (dashed outline, Figure 15). If correct, this would predict that the rake of the 1986 slip vector changes from relatively more oblique to relatively more strike slip from west to east, respectively. Whether first motion solutions of the aftershocks reflect this change is not known.

7. Tests of the Concept

[70] The three-dimensional geometry that we propose for the San Andreas fault zone through the San Gorgonio Pass stepover has implications for the geologic history of the region. If the San Gorgonio Pass-Garnet Hill fault were to have formed the entire 5–8 km high seismicity step as an offset, total uplift across the faults would have to equal 5–8 km. This is inconsistent with the geologic history of these faults. Total slip across the Garnet Hill and SGPFs is almost certainly too small and their history too short [*Matti and Morton*, 1993] to account for the entire 5–8 km high step in seismicity. Furthermore, these faults have not been active long enough to have accrued such large offsets, even if they were to have carried the entire 25 mm/yr of the entire San Andreas fault zone during their short lifetimes. Near-surface vertical offsets across these two faults are probably no more than about 1 km, and they have probably not been active for more than a 125,000 years or so [*Matti and Morton*, 1993].

[71] To create the entire seismic step by offset on reverse faults, the currently inactive reverse faults farther north would need to be called upon. Figure 16 consists of a cross section across the faults, the seismicity step, and related structures. It shows that vertical offset across the entire system of faults could be as great as about 3–5 km, about 50–75% of what would be needed to account for the step in seismicity. We estimated this vertical offset by projecting the Miocene nonconformity, dipping about 15°–20° toward the east in the Whitewater Canyon area [*Allen*, 1957], westward to the line of cross section (Figure 16). Much if not all of the slip on these faults occurred after deposition of the late Pliocene Painted Hill Formation, and perhaps as recently as after the deposition of the late Pleistocene Cabezon Formation.

[72] We do not consider the apparent shortfall in the vertical offset near the surface across the San Gorgonio and Banning faults to be a flaw in the model. Rather, as *Magistrale and Sanders* [1996] concluded, a rheological difference in basement rocktypes at depth can explain the remainder of the step in seismicity, with relatively weak quartz-rich crust on the north (Pelona schist) and relatively strong feldspar-rich rocks on the south (Peninsular Ranges batholith). A combination of vertical offset and rheologic differences across the SGPF can therefore account for the 5–8 km seismicity step (Figure 13). Furthermore, we show Pelona schist at a depth of 8–10 km beneath the San Bernardino Mountains (to the north of the Mill Creek fault). This not only explains the unusually shallow seismicity there [*Magistrale and Sanders*, 1996], but might represent the detachment surface proposed by *Hadley and Kanamori* [1977] and *Nicholson et al.* [1986] for this depth in the San Gorgonio Pass region.

8. Implications for Future Ruptures

[73] We have proposed a structural model, modified from the work of *Allen* [1957], *Matti et al.* [1992a], and *Matti and Morton* [1993], that involves a gradual northwestward transformation of the San Andreas fault from a near-vertical strike-slip fault (in the southeastern Coachella Valley) into a shallow-dipping, oblique-reverse fault (along the southern margin of the San Bernardino Mountains). In contrast, the

joint between the near-vertical strike-slip San Bernardino strand of the fault and the oblique-reverse segment is abrupt. What are the implications of this structural model for future large earthquakes there?

[74] First, it defines a plausible geometry for future earthquake sources. This is a critical initial step in modeling the seismic energy released by rupture of the various fault planes. Table 1 shows the area of the active fault planes we have mapped and extrapolated to depth. Average displacements are approximate and depend on poorly constrained slip rates. In addition, our model provides crude characterization of the slip vectors we would expect on the various seismic sources.

[75] Second, it provides a better basis for quantitative modeling of dynamic rupture propagation through the fault zone in this region. Can ruptures propagate through, or is this a ''knot'' as suggested by *Sykes and Seeber* [1985]. A rupture of some or all of the faults in the pass region would likely produce rupture delays at stepovers, similar to those observed during the Landers quake [*Wald and Heaton*, 1994].

[76] Third, it provides a starting point for analysis of the partitioning of 20–25 mm/yr through the region on the various faults, by rotations, and by folding. Slip-rate studies can test hypotheses implicit in our model, such as the transfer of slip off the Coachella Valley strand of the Banning fault and onto the Garnet Hill fault. Individual ruptures must sum to create the cumulative neotectonic motions. But once slip and rotation rates are known, we can construct scenario events for this section of the fault zone that will include the lesser normal-oblique faults and folds.

[77] Fourth, our structural model provides a context in which to understand paleoseismic data, which could be one of the arbiters of whether or not the several faults move in conjunction or separately. Does the structurally complex San Gorgonio Pass region block or inhibit throughgoing rupture [*Sykes and Seeber*, 1985]? Paleoseismic data permit the correlation of certain events reported from sites between Pallett Creek on the northwest and Indio on the southeast, over a distance of about 200 km [*Sieh and Jahns*, 1984; *Sieh et al.*, 1989; *Seitz et al.*, 1997; *Fumal et al.*, 1993; *Yule et al.*, 2001]. This suggests that the San Andreas fault system in San Gorgonio Pass might rupture in relatively infrequent large (*M*8) earthquakes from the Coachella Valley to the Mojave Desert, contradictory to the concept of a restraining bend acting as an impediment to throughgoing rupture.

[78] **Acknowledgments.** Our work in San Gorgonio Pass began in the late 1980s and early 1990s as a series of mapping exercises for undergraduate and graduate students. Later work was supported by the Southern California Earthquake Center (SCEC). SCEC is funded by NSF Cooperative Agreement EAR-8920136, USGS Cooperative Agreements 14-08-0001-A0899 and 1434-HQ-97AG01718. A portion of our work was also funded through SCEC by Pacific Gas and Electric. Thorough and constructive critiques were provided by *Journal of Geophysical Research* reviewers Jon Matti and Harold Magistrale. Early drafts benefited from reviews and conversations with Andrew Meigs, Jim Spotila, Anke Friederich, Yann Klinger, Jing Liu, and an initial GIS compilation of our data by Tony Soeller. We appreciate the cooperation and support of the Morongo Band of Mission Indians. Harold Magistrale generously provided hypocentral locations for microearthquakes in the San Gorgonio Pass region for the years 1981–1993. Jon Matti and Doug Morton kindly provided copies of unpublished geologic maps of the Cabazon and Whitewater 7.5' quadrangles. We are grateful to Richmond Wolf for providing us with his preliminary geologic maps of the Whitewater Hill-Garnet Hill region. Arnie N. Clyde enthusiastically provided field assistance. This is SCEC contribution no. 709 and Caltech Seismological Laboratory contribution no. 8981.

References

Ague, J., and M. Brandon, Tilt and northward offset of Cordilleran batholiths resolved using igneous barometry, *Nature*, *360*, 146–149, 1992.

Allen, C., San Andreas fault zone in San Gorgonio Pass, southern California, *Geol. Soc. Am. Bull.*, *68*, 315–350, 1957.

Anderson, R., Evolution of the Santa Cruz Mountains, California, through tectonic growth and geomorphic decay, *J. Geophys. Res.*, *99*, 20,161–20,180, 1994.

Barka, A., and K. Kadinsky-Cade, Strike-slip fault geometry in Turkey and its influence on earthquake activity, *Tectonics*, *7*, 663–684, 1988.

Cisternas, A., et al., The Spitak (Armenia) earthquake of 7 December 1988: Field observations, seismology, and tectonics, *Nature*, *339*, 675–679, 1989.

Clark, M., Map showing recently active breaks along the San Andreas fault and associated faults between the Salton Sea and Whitewater River-Mission Creek, California, *Misc. Geol. Invest. Map, I-1483*, U.S. Geol. Surv., Boulder, Colo., 1984.

Dibblee, T., Geologic map of the San Gorgonio Mountain 15′ quadrangle, San Bernardino and Riverside counties, scale 1:62,500, *Misc. Geol. Invest. Map, I-517*, U. S. Geol. Surv., Boulder, Colo., 1964.

Dibblee, T., Displacements on San Andreas fault system in San Gabriel, San Bernardino, and San Jacinto Mountains, southern California, in *Proceedings of Conference on Geologic Problems of San Andreas Fault System*, edited by W. R. Dickinson and A. Grantz, pp. 260–278, Stanford Univ. Press, Stanford, Calif., 1968.

Dibblee, T., Regional geologic map of San Andreas and related faults in eastern San Gabriel Mountains, San Bernardino Mountains, western San Jacinto Mountains and vicinity, Los Angeles, San Bernardino, and Riverside counties, California, *Open File Map*, U. S. Geol. Surv., Boulder, Colo., 1970.

Dibblee, T., Late quaternary uplift of the San Bernardino Mountains on the San Andreas and related faults, *Spec. Rep. Calif. Div. Mines Geol.*, *118*, 127–135, 1975.

Dibblee, T., Geology of the San Bernardino Mountains, southern California, in *Geology and Mineral Wealth of the California Transverse Ranges*, *South Coast Geol. Soc. Guideb.*, vol. 10 (Mason Hill volume), edited by D. L. Fife and J. A. Minch, pp. 148–169, South Coast Geol. Soc., Santa Ana, Calif., 1982.

Fumal, T., S. Pezzopane, I. R. Weldon, and D. Schwartz, A 100-year average recurrence interval for the San Andreas fault at Wrightwood, California, *Science*, *259*, 199–203, 1993.

Hadley, D., and H. Kanamori, Seismic structure of the Transverse Ranges, California, *Geol. Soc. Am. Bull.*, *88*, 1469–1478, 1977.

Harden, J., and J. Matti, Holocene and late Pleistocene slip rates on the San Andreas fault in Yucaipa, California, using displaced alluvial-fan deposits and soil chronology, *Geol. Soc. Am. Bull.*, *101*, 1107–1117, 1989.

Harris, R., and S. Day, Dynamics of fault interaction: Parallel strike-slip faults, *J. Geophys. Res.*, *98*, 4461–4472, 1993.

Hartzell, S., Comparison of seismic waveform inversion results for the rupture history of a finite fault: Application to the 1986 North Palm Springs, California, earthquake, *J. Geophys. Res.*, *94*, 7515–7534, 1989.

Hill, M., Anomalous trends of the San Andreas fault in the Transverse Ranges, California, in *Geology and Mineral Wealth of the California Transverse Ranges*, edited by D. L. Fife and J. A. Minch pp. 367–369, South Coast Geol. Soc., Santa Ana, Calif., 1982.

Jones, L., L. Hutton, D. Given, and C. Allen, The North Palm Springs, California, earthquake sequence of July 1986, *Bull. Seismol. Soc. Am.*, *76*, 1830–1837, 1986.

Keller, E., M. Bonkowski, R. Korsch, and R. Shiemon, Tectonic geomorphology of the San Andreas fault zone in the southern Indio Hills, Coachella Valley, California, *Geol. Soc. Am. Bull.*, *93*, 46–56, 1982.

Lisowski, M., W. Prescott, J. Savage, and M. Johnston, Geodetic estimate of coseismic slip during the 1989 Loma Prieta, California, earthquake, *Geophys. Res. Lett.*, *17*, 1437–1440, 1990.

Magistrale, H., and C. Sanders, Evidence from precise earthquake hypocenters for segmentation of the San Andreas fault in San Gorgonio Pass, *J. Geophys. Res.*, *101*, 3031–3041, 1996.

Marshall, G., R. Stein, and W. Thatcher, Faulting geometry and slip from co-seismic elevation changes: The 18 October 1989, Loma Prieta, California, earthquake, *Bull. Seismol. Soc. Am.*, *81*, 1660–1693, 1991.

Matti, J., and D. Morton, Paleogeographic evolution of the San Andreas fault in southern California: A reconstruction based on a new cross-fault correlation, *Geol. Soc. Am. Mem.*, *178*, 107–159, 1993.

Matti, J., D. Morton, and B. Cox, Distribution and geologic relations of fault systems in the vicinity of the central Transverse Ranges, southern

California, *U.S. Geol. Surv. Open File Rep. 85-365*, scale 1:25,0000, 27 pp., U.S. Geol. Surv., Reston, Va., 1985.

Matti, J., D. Morton, and B. Cox, The San Andreas fault system in the vicinity of the central Transverse Ranges province, southern California, *U.S. Geol. Surv. Open File Rep., 92-354*, 40 pp., U.S. Geol. Surv., Reston, Va., 1992a.

Matti, J., D. Morton, B. Cox, S. Carson, and T. Yetter, Geologic map of the Yucaipa 7.5′ quadrangle, California, *U.S. Geol. Surv. Open File Rep., 85-446*, 14 pp., U.S. Geol. Surv., Reston, Va., 1992b.

Morton, D., J. Matti, and J. Tinsley, Banning fault, Cottonwood canyon, San Gorgonio pass, southern California, in *Cordilleran Section of the Geological Society of America*, edited by M. Hill, pp. 191–192, Geol. Soc. of Am., Boulder, Colo., 1987.

Morton, D. M., and J. C. Matti, Extension and contraction within an evolving divergent strike-slip fault complex: The San Andreas and San Jacinto fault zones at their convergence in southern California, *Geol. Soc. Am. Mem.*, *178*, 217–230, 1993.

Nicholson, C., Seismic behavior of the southern San Andreas Fault Zone in the Northern Coachella Valley, California: Comparison of the 1948 and 1986 earthquake sequences, *Bull. Seismol. Soc. Am.*, *86*, 1331–1349, 1996.

Nicholson, C., L. Seeber, P. Williams, and L. R. Sykes, Seismicity and fault kinematics through the eastern Transverse Ranges, California: Block rotation, strike-slip faulting and shallow-angle thrusts, *J. Geophys. Res.*, *91*, 4891–4908, 1986.

Noble, L. F., The San Andreas rift and some other active faults in the desert region of southeastern California, *Year Book Carnegie Inst. Washington*, *25*, 415–435, 1926.

Noble, L. F., The San Andreas rift in the desert region of southeastern California, *Year Book Carnegie Inst. Washington*, *31*, 355–363, 1932.

Rasmussen, G., and W. Reeder, What happens to the real San Andreas fault at Cottonwood canyon, San Gorgonio pass, California?, in *Geology Around the Margins of the Eastern San Bernardino Mountains*, edited by M. A. Kooser and R. E. Reynolds, pp. 157–162, Inland Geol. Soc., Redlands, Calif., 1986.

Rice, J., and Y. Ben-Zion, Slip complexity in earthquake fault models, *Proc. Natl. Acad. Sci. U. S. A.*, *93*, 3811–3818, 1996.

Sadler, P. M., and W. A. Reeder, Upper Cenozoic, quartzite-bearing gravels of the San Bernardino Mountains, southern California; recycling and mixing as a result of transpressional uplift, in *Tectonics and Sedimentation Along Faults of the San Andreas System*, edited by D. W. Anderson and M. J. Rymer, pp. 45–57, Pac. Sect., Soc. of Econ. Paleontol. and Min., Los Angeles, Calif., 1983.

Sadler, P. M., A. Demirer, D. West, and J. M. Hillenbrand, The Mill Creek basin, the Potato sandstone, and fault strands in the San Andreas fault south of the San Bernardino Mountains, *Geol. Soc. Am. Mem.*, *178*, 289–306, 1993.

Seeber, L., and J. Armbruster, The San Andreas fault system through the Transverse Ranges as illuminated by earthquakes, *J. Geophys. Res.*, *100*, 8285–8310, 1995.

Seitz, G., R. Weldon, and G. P. Biasi, The Pitman Canyon paleoseismic record: A re-evaluation of southern San Andreas fault segmentation, *J. Geodyn.*, *24*, 129–138, 1997.

Sieh, K., Slip along the San Andreas fault associated with the great 1857 earthquake, *Seismol. Soc. Am. Bull.*, *68*, 1421–1428, 1978.

Sieh, K., and R. H. Jahns, Holocene activity of the San Andreas Fault at Wallace Creek, California, *Geol. Soc. Am. Bull.*, *95*, 883–896, 1984.

Sieh, K., and J. C. Matti, The San Andreas fault system between Palm Springs and Palmdale, southern California: Field trip guidebook, in *Earthquake Geology San Andreas Fault System Palm Springs to Palmdale*, pp. 1–12, Assoc. of Eng. Geol., South. Calif. Sec., 1992.

Sieh, K., and D. Natawidjaja, Neotectonics of the Sumatran fault, Indonesia, *J. Geophys. Res.*, *105*, 28,295–28,326, 2000.

Sieh, K., M. Stuiver, and D. Brillinger, A more precise chronology of earthquakes produced by the San Andreas fault in southern California, *J. Geophys. Res.*, *94*, 603–623, 1989.

Sieh, K., et al., Near-field investigations of the Landers earthquake sequence, April to July 1992, *Science*, *260*, 171–176, 1993.

Spotila, J., K. Farley, and K. Sieh, Uplift and erosion of the San Bernardino Mountains associated with transpression along the San Andreas fault, California, as constrained by radiogenic helium thermochronometry, *Tectonics*, *17*, 360–378, 1998.

Spotila, J., K. Farley, D. Yule, and P. Reiners, Near-field transpressive deformation along the San Andreas fault zone in southern California, based on exhumation constrained by (U-Th)/He dating, *J. Geophys. Res.*, *106*, 30,909–30,922, 2001.

Sykes, L., and L. Seeber, Great earthquakes and great asperities, San Andreas fault, southern California, *Geology*, *13*, 835–838, 1985.

van der Woerd, J., Y. Klinger, K. Sieh, P. Tapponier, and F. Reyerson, First long-term slip-rate along the San Andreas fault based on 10-Be-26Al surface exposure dating: The Biskra Palms site, 22 mm/yr for the last 30,000 years, *Eos Trans. AGU*, *82*(47), Fall Meet. Suppl., F934, 2001.

Vaughan, F., Geology of the San Bernardino Mountains north of San Gorgonio Pass, *Univ. Calif. Dept. Geol. Sci. Bull.*, *13*, 319–411, 1922.

Wald, D., and T. Heaton, Spatial and Temporal Distribution of Slip for the 1992 Landers, California, Earthquake, *Seismol. Soc. Am. Bull.*, *84*, 668–691, 1994.

Weldon, R., and K. Sieh, Holocene rate of slip and tentative recurrence interval for large earthquakes on the San Andreas fault, Cajon Pass, southern California, *Geol. Soc. Am. Bull.*, *96*, 793–812, 1985.

Wesnousky, S., and C. Jones, Oblique slip, slip partitioning, spatial and temporal changes in the regional stress field, and the relative strength of active faults in the Basin And Range, western United States, *Geology*, *22*, 1031–1034, 1994.

Wolf, R., K. Farley, and L. Silver, Assessment of (U-Th)/He thermochronometry: The low-temperature history of the San Jacinto Mountains, California, *Geology*, *25*, 65–68, 1997.

Yeats, R., Active faults related to folding, in *Active Tectonics*, edited by R. Wallace, pp. 63–79, Natl. Acad. Press, Washington, D. C., 1986.

Yule, J., T. Fumal, S. McGill, and G. Seitz, Active tectonics and paleoseismic record of the San Andreas fault, Wrightwood to Indio: Working toward a forecast for the next "Big Event," in *Geologic Excursions in the California Deserts and Adjacent Transverse Ranges*, edited by G. Dunne and J. Cooper, pp. 91–126, Pac. Sect., Soc. of Econ. Paleontol. and Min., Los Angeles, Calif., 2001.

K. Sieh, Seismological Laboratory, California Institute of Technology, Pasadena, CA 91125, USA.

D. Yule, Department of Geological Sciences, California State University, Northridge, CA 91330-8266, USA. (j.d.yule@csun.edu)